Tome 7 *Novembre 1969* Numéro 4

うみ

La mer

昭和 44 年 11 月

日 仏 海 洋 学 会

La Société franco-japonaise
d'océanographie
Tokyo, Japon

投 稿 規 定

1. 報文の投稿者は原則として本会会員に限る。
2. 原稿は簡潔にわかりやすく書き，図表を含めて印刷ページで12ページ以内を原則とする。原稿は，東京都千代田区神田駿河台 2-3　日仏会館内　日仏海洋学会編集委員会宛に送ること。
3. 編集委員会は，事情により原稿の字句の加除訂正を行なうことがある。
4. 論文には必ず約 500 字の和文の要約をつけること。
5. 図および表は必要なもののみに限る。図はそのまま版下になるように縮尺を考慮して鮮明に黒インクで書き，論文の図および表には必ず英文（または仏文）の説明をつけること。
6. 初校は原則として著者が行なう。
7. 報文には 1 編につき50部の別刷を無料で著者に進呈する。これ以上の部数に対しては，実費（送料を含む）を徴収する。

RECOMMANDATIONS A L'USAGE DES AUTEURS

1. Les auteurs doivent être, en principe, des Membres de la Société franco-japonaise d'océanographie. Néanmoins, les notes des savants étrangers à la Société seront acceptées, si elles sont présentées par un Membre.
2. Les notes ne peuvent dépasser douze pages. Les manuscrits, dactylographiés sur papier fort, doivent être envoyés au Comité de rédaction de la Société franco-japonaise d'océanographie, c/o Maison franco-japonaise, 2-3 Kanda, Surugadai, Chiyoda-ku, Tokyo.
3. Le Comité de rédaction se réserve le droit d'apporter, le cas échéant, des modifications mineuses aux manuscrits ainsi que de demander aux auteurs de les corriger.
4. Des résumés en langue japonaise ou langue française sont obligatoires.
5. Les figures au trait seront tracées à l'encre de Chine noire sur papier blanc ou sur calque. Les légendes des figures et des tableaux sont indispensables.
6. Les premières épreuves seront corrigées, en principe, par les auteurs.
7. Un tirage à part des articles en cinquante exemplaires est offert gratuitement aux auteurs. Ceux qui en désirent un plus grand nombre peuvent les faire établir à leurs frais.

La mer (Bulletin de la Société franco-japonaise d'océanographie)
Tome 7, N° 4, Novembre 1969)

日本海における鉄・アルミニウムの分布とその海洋学的意義*
—(第2報) 東支那海およびオホーツク海との関係

杉 浦 吉 雄** 山 本 克 己***

The Distribution of Iron and Aluminum in Sea Water of the Japan Sea and its Oceanographical Significance
— (2) The Relation of the Japan Sea with the East China Sea and the Okhotsk Sea

Yoshio SUGIURA and Katsumi YAMAMOTO

Abstract: Taking both concentrations of iron and aluminum with chlorinity into account, the following points have been pointed out:

(1) The surface water of the northern side of the Japan Sea is a (1:1) mixture of Okhotsk water and Tsushima warm current water.

(2) The Tsushima warm current water is not the same as the Kuroshio water occupying the sea area south of the Kyushu Island, but that influenced by the continental run-off at or around the Tsushima Straits.

1. はしがき

著者ら(杉浦,山本,1968)[1]は,さきに,日本海における海水の鉄(Fe)とアルミニウム(Al)の分布について,次の点を明らかにした。(1) Fe, Al の濃度にはムラがあるから,分布を論ずる場合には,ある程度の広がりをもつ海域について平均濃度と偏差を求めて,相互に比較することが有効である。この点は,塩素量(Cl)と異なる。表層(200 m 以浅),中層(200～500 m)深層(500 m 以深)に区分すると,平均濃度も標準偏差もこの順に低下する。(3) 三つの層を問わず,本州寄り(南側)では大陸寄り(北側)より平均濃度も標準偏差も大きい。(4) 南北いずれにおいても,東西間に濃度の差がある。表層については,南側では西高東低,北側ではその逆である。Cl については,南北の差ほど東西間の差は大きくない。中層の分布は,表層に似ているが,深層では南側で東高西低である。(5) 北側東部では,表層よりかえって中層において濃度がいくぶん高い。(6) 以上 (1)～(5) の結果は,Fe, Al が海水中で粒子状に存在し,重力による沈降が現象を支配すること,対馬海峡以西,津軽あるいは宗谷海峡以東に Fe, Al の供給源があることを仮定すると,よく説明できる。

(6) の指摘に基づいて,東支那海とオホーツク海における海水の Fe, Al 濃度を測定し,日本海の海水の Fe, Al 濃度との関係を究明した。その結果について以下に述べる。

2. オホーツク海における海水中の Fe, Al

Fig. 1 は,採水点を示す。観測は,1968年6月20日より7月1日までの間に行なった。図では,各測点の脇に海底までの深さを示す。カムチャッカ半島にもっとも近い点で 900 m,他は 3,000 m 内外である。表層(200 m 以浅),中層(200～500 m),深層(500 m 以深)に区分し,それぞれにおける平

* 1969年7月4日受理
** 気象研究所 Meteorological Research Institute
*** 神戸海洋気象台 Kobe Marine Observatory

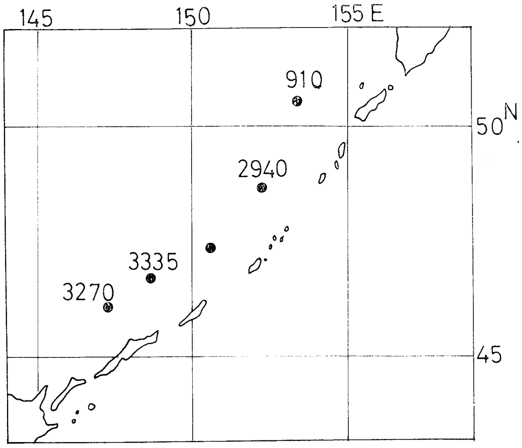

Fig, 1. The location of stations in the Okhotsk Sea. A figure aside each station shows the depth in meters.

均濃度と標準偏差を示すと，Table 1 のようになる。

Table 1 は，Al, Fe 濃度が平均値についても標準偏差についても，大体，深度とともに減少の傾向にあることを示している。Table 1 のオホーツク海の水は，日本海の南側より北側の水と，Al, Fe の濃度において似ている。一方，塩素量をみると，日本海の北側では，深さ 50 m で平均 18.8 ‰ であるのに，オホーツク海では，18.4 ‰ 以下と低い。従って，オホーツク海の水がそのまま日本海の北側の水を形成するとは考えられない。いま，19.08 ‰ の対馬暖流水に 18.4 ‰ のオホーツク海の水が混合した結果 18.8 ‰ の日本海の北側の水が生じたとしよう。6 割の対馬暖流水が 4 割のオホーツク海の水と混合すればよい。Fe, Al については，日本海の南側東部における Fe, Al 濃度の 6 割とオホーツク海の Fe, Al 濃度の 4 割を加算して，Al 32, Fe 22 μg/l の値を得る。一方，日本海北側東部における Al, Fe 濃度の観測値は，それぞれ，29, 21 μg/l である。これは，日本海の北側表層水が，対馬暖流水とオホーツク海の水の等量混合水に近いことを示唆するものである。

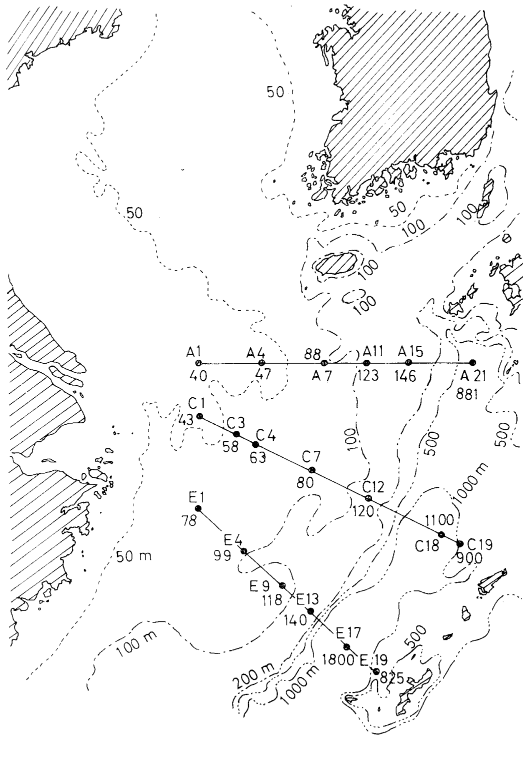

Fig. 2. The location of stations and the topography in the East China Sea. A figure aside station shows the depth in meters. A figure aside each isobath shows the depth in meters.

Table 1. Averages and standard deviations of Al and Fe concentrations in sea water of the southern part of the Okhotsk Sea.

Layer	Surface	Intermediate	Deep
Depth (m)	<200	200～500	>500
Al, μg/l	22.8± 9.02(33)*	23.7± 6.92(18)	20.9±5.61(35)
Fe, μg/l	23.4±13.90(33)	19.0±10.63(18)	17.8±5.46(35)

* Figures in parentheses show number of samples.

3. 東支那海における海水中の Fe, Al

Fig. 2 は採水点を示す。観測は，1968 年 10 月 12～15 日に，凌風丸，長風丸，清風丸で同時に平行して行なわれた。図では，各点の脇に海底までの深さを示す。Figs. 3～5 は，海底から上向きに測った深さに対して，Al, Fe の濃度をプロットしたものである。これによって，海底直上 50 m くらいから海底に接近するほど，Al, Fe の濃度が増加する傾向にあることがわかる。これは，海底からの巻き上り効果と考えられる。図の白丸は Cl < 19.0 ‰，黒丸は Cl ≧ 19.0 ‰ の水を表わす。それぞれの直線，破線で結ばれた丸は，同一観測点での値を示す。海底直上の水の塩素量が 19.0 ‰ 以下のとき，巻き上り効果がとくに顕著である。A, C 線に比べると，E 線における陸水の影響は少い。Figs. 3～5 が指摘する傾向のあるものは，次の Table 2 によってさらに明瞭である。

Table 2 によれば，海底から 50 m 以内の水で Cl < 19.0 ‰ の場合が，Al, Fe の高濃度の出現確率において，もっとも高い。このような水は，揚子江の河口に近い場所で発見される。これに対して，海底から 50 m 以上距たる深さの水は，Cl の値にかかわらず Al, Fe の高濃度出現確率が低い。ことに，Cl ≧ 19.0 ‰ の黒潮水が，日本海の対馬暖流域の表層水に比べて低いことは，注目に値する。これによって，九州南方の黒潮水がそのまま日本海の対馬暖流水になるわけではないことがわかる。また，海底から 50 m 以上距たる深さにあって，海面下 200 m 以浅の水が，Cl < 19.0 ‰ すなわち，陸水の影響を受けていると思われる条件下にありながら，日本海の対馬暖流水に比べてかなり低い Fe, Al 濃度を示すことは，注目に価する。

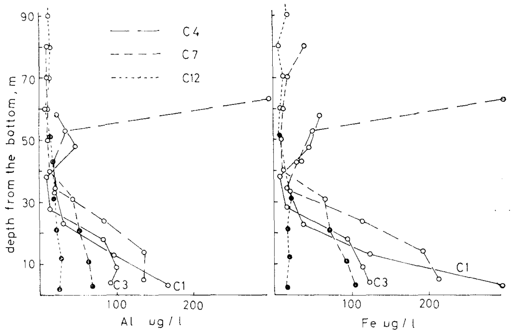

Fig. 4. The vertical distribution of iron and aluminum above the bottom on the C-line in the East China Sea.

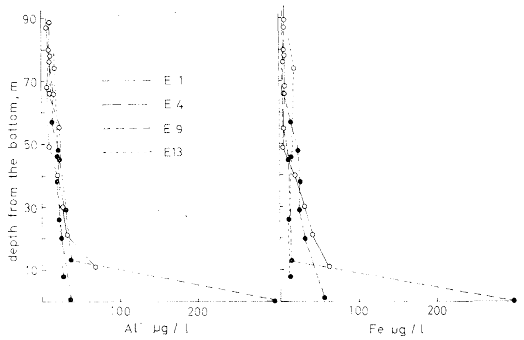

Fig. 5. The vertical distribution of iron and aluminum above the bottom on the E-line in the East China Sea.

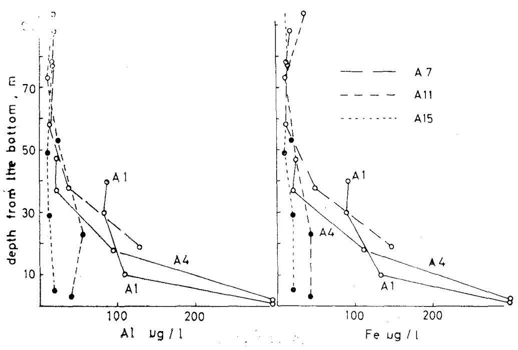

Fig. 3. The vertical distribution of iron and aluminum above the bottom on the A-line in the East China Sea.

対象海域の大陸棚上では，大陸から放出される Fe, Al を含む粒子が比較的はやく沈降して，海底上 50 m 以上距たる層から失われていると考えられる。

一方，海底上 50 m 以内にあって Cl ≧ 19.0 ‰ の水が，Al, Fe の高濃度出現確率において，対馬暖流水に匹敵する点に着目すると，元来，Fe, Al 含量の低い黒潮水でも，海底付近では Fe, Al 濃度を増し得ることがわかる。対馬海峡は，大部分が深さ 100 m 内外の浅瀬であるから，ここに押し寄

Table 2. Frequency of occurrence of water having the concentration within each range for waters occupying within and beyond 50 m above the bottom. In the case of the depth beyond 200 m, the layer shallower than the depth of 200 m from the surface is only considered.

Conc'n range Al or Fe μg/l	Within 50 m above the bottom		Beyond 50 m above the bottom		Southern side of Japan Sea
	Cl ≥ 19.0 ‰	Cl < 19.0 ‰	Cl ≥ 19.0 ‰	Cl < 19.0 ‰	
Al					
0— 10	0	0	0	7	0
10— 20	3	7	21	32	23
20— 30	11	5	16	8	40
30— 40	3	3	2	3	14
40— 50	1	2	0	0	8
50— 60	2	0	0	0	4
60— 70	1	1	0	0	2
70— 80	1	0	0	0	0
80— 90	0	4	0	0	1
90—100	0	3	0	1	3
100—150	0	5	0	0	10
150—200	0	1	1	0	3
>200	1	2	0	1	1
Total	23	33	40	52	109
Average, μg/l	31.1	60.4	27.9	17.5	45.8
Standard deviation	16.33	45.02	27.07	12.44	42.07
Fe					
0— 10	0	2	5	17	24
10— 20	8	4	22	24	44
20— 30	7	1	8	5	13
30— 40	1	4	3	1	9
40— 50	2	3	1	1	6
50— 60	1	0	0	2	2
60— 70	0	2	0	1	2
70— 80	1	0	0	0	1
80— 90	0	0	0	0	3
90—100	1	3	0	0	2
100—150	1	6	0	0	5
150—200	0	1	0	0	0
>200	1	3	1	1	1
Total	23	29	40	52	112
Average, μg/l	32.0	80.8	22.0	16.2	29.5
Standard deviation	26.68	84.38	29.26	12.74	33.44

せる黒潮の水は，あたかも大陸棚上の前記底層水のように，Fe, Al 濃度を増す可能性が考えられる。ただし，日本海に流亡する Fe, Al を常に補充する機構が一方ではなければならない。前述のように，Fe, Al の大陸棚上での挙動をみると，高い濃度は，海底上 50 m 以内の層に限られる。従って，高濃度の伝達機構としては，海底上 50 m 程度の厚さの層の中で，深さ 100 m 内外の大陸棚上を，拡散や流れによって，大陸沿岸から対馬海峡に Fe, Al を運ぶ比較的塩分の低い水が，海峡近くで黒潮と接触し，これに Fe, Al の高濃度を伝達することが考えられる。この仮説の当否は，今後，

対馬海峡と黄海の観測によって，検討されなければならない。

4. むすび

海水中の Fe, Al 濃度と Cl を合わせ考えると，日本海の大陸寄り表層水は，オホーツク海の水と対馬暖流水のおよそ (1:1) の混合水であることがわかる。一方，日本海の本州寄りを流れる対馬暖水流は，九州南方域を占める黒潮水そのものではなく，対馬海峡あるいはその周辺で大陸の影響を強く受けた黒潮水であることが考えられる。ただし，後の点については，今後，観測域を黄海，対馬海峡まで拡げて確かめる必要がある。

文　　献

1) 杉浦吉雄，山本克己 (1968): 日本海における鉄，アルミニウムの分布とその海洋学的意義. うみ, **6** (3), 177–189.

La mer (Bulletin de la Société franco-japonaise d'océanographie)
Tome 7, N° 4, Novembre 1969

On the Oxygen Consumption Accomanying the Biochemical Decomposition and Oxidation of Nitrogenous Organic Matter in Sea Water*

Keinosuke MOTOHASHI** and Chikayoshi MATSUDAIRA**

Abstract: The oxygen consumption accompanying the biochemical decomposition and oxidation of the diatom *Skeletonema costatum* which was chosen as a source of nitrogenous organic matter in sea water has been reproduced experimentally in the dark at both temperatures of 20°C and 30°C.

The biochemical decomposition of particulate-nitrogen in sea water was commenced immediately after the storage in the dark. The amount of 60 to 70 per cent of it was easily decomposed and the residual fractions were hard to be affected by biochemical decomposition. Ammonium-nitrogen appeared in water rapidly at the beginning of the biochemical decomposition of particulate-nitrogen, and its concentration reached the maximum when the biochemical decomposition of particulate-nitrogen almost finished. The time lag in the oxidation of ammonia to nitrite and finally nitrate was apparently recognized among both temperatures and the total duration of the different forms of nitrogen appeared by biochemical decomposition and oxidation of nitrogenous organic matter differed at both temperatures.

A period of oxygen consumption accompanying biochemical decomposition and oxidation of nitrogenous organic matter was subdivided into two phases: an exponential phase and a linear phase. The time which shifted from an exponential phase to a linear phase corresponded just to the maximum concentration of ammonia and/or the end of the biochemical decomposition of particulate-nitrogen.

Between ammonia-N, nitrite-N, and nitrate-N produced by biochemical decomposition and oxidation of nitrogenous organic matter and oxygen consumption in their oxidation there was a fair correlation, which was linear. It might be inferred from the present study that below the euphotic zone in open ocean the biochemical oxidation of ammonia to nitrite and finally to nitrate would be to proceed while certain constant ratios for the oxygen consumption are kept.

1. Introduction

The nitrogenous compounds in actual sea water exist in the following different forms such as ammonium-nitrogen, nitrite-nitrogen, nitrate-nitrogen, dissolved organic nitrogen, and particulate-nitrogen. These forms play an important role as main plant nutrient in the same way as phosphorus compounds for the primary production in the ocean, and are also generally considered to be the limiting factor for the growth of marine phytoplankton.

So far, the uptake of nitrogen compounds from sea water by diatom and the regeneration from nitrogenous organic matter decomposing in sea water have been studied by several groups of researchers. COOPER (1937) discussed in detail the nitrogen cycle in the sea using the thermodynamics extensively. Based on this classical contribution, VON BRAND *et al.* reported a series of heroic researches concerning biochemical decomposition and regeneration of nitrogenous organic matter in sea water in the second half of 1930 and in the first half of 1940 (VON BRAND *et al.*, 1937, 1939, 1940, 1941 and 1942). These same authors have reproduced the nitrogen cycle experimentally and classified it into the main stages according to the following scheme: living organism–dead organism–ammonia–nitrite–nitrate

* Received August 27, 1969
** Department of Fisheries, Faculty of Agriculture, Tohoku University

-living organism.

Recently several works on such biochemical decomposition and regeneration of nitrogenous compounds were carried out, *in vitro*, by GRILL and RICHARDS (1963) and KAMATANI (1968). Most of them have dealt under an experimental condition of high organic nitrogen concentrations which is far different from the natural sea water. On the other hand, concerning biochemical decomposition and regeneration of nitrogenous compounds *in situ* we may refer to the following contributions by HARRIS (1959) in the Long Island Sound Water, VACCARO and RYTHER (1960), VACCARO (1963) in the Atlantic off New England, and HAMILTON (1964). From the above works the oxidation of ammonia to nitrite and finally to nitrate was expected to be caused by the following three factors; (1) photochemical oxidation, which is limited at the sea surface, (2) biochemical oxidation in the presence of dissolved oxygen and (3) bacterial activity. On the whole, biochemical decomposition and regeneration of nitrogenous compounds in sea water are proceeded maily under combined processes of biochemical oxidation and bacterial activity in the presence of dissolved oxygen. Therefore, the information as to the correlation between oxygen consumption and nutrient regeneration from orgrnic matter decomposing in sea water has an important meaning on the explanation of the relation between biochemical activity and relative composition of nutrients in the ocean. Furthermore, this correlation is becoming important for many theoretical and applied problems in the estimation of primary production and in investigation of the distribution of oxygen in the ocean. Nevertheless, several groups of researchers up to the present have dealt only with the comprehensive nutrient regeneration from organic matter decomposing in sea water. There have been very few contributions which have dealt with the oxygen consumption as a result of biochemical decomposition and oxidation of organic matter up to the present with the exception of observations by the present authors (1969a, '69b, and '69c), which have dealt with some works on the oxygen consumption accompanying the biochemical oxidation of phosphorous compounds in sea water.

In the present paper the authors deal first with the rate and extent of the regeneration of different forms of nitrogen from phytoplankton decomposing in sea water at different temperatures and next obtain the correlation between different forms of nitrogen and oxygen consumption accompanying the biochemical oxidation thereof.

2. Experimental procedure

The sea water used in this experiment was collected from Yoshida-Hama, Miyagi Prefecture where relatively uncontaminated sea water could be obtained, and brought into the laboratory. It was filtered through commercial cotton, and the nutrients were added to it at the concentration of 150 μg PO_4-P, 1,050 μg NO_3-N, 1,500 μg SiO_2-Si, and 0.5 μg vitamin B_{12}, per liter. Sterilization was achieved in the autoclave for an hour at ca. 100°C. After cooling at a room temperature, the artificial culture of diatom *Skeletonema costatum* **(Greville) Cleve** was chosen as a source of nitrogenous organic matter, which was inoculated in the above sterilized medium. The sample was exposed to daylight-type fluorescent lamp that gave a total illumination of about 10,000 lux. The detailed procedure of diatom culture has been described in the previous reports (MOTOHASHI and MATSUDAIRA, 1969a, '69b). When the inorganic phosphate concentration in medium was reduced to a trace after inoculation, it was put aside for several days. The light was thereafter removed and the sample was diluted with non-sterilized and filtered sea water as the same as used in the above medium. The diluted sample was bubbled with oxygen gas for a while, and then the diluted mother sample was siphoned into glass-stoppered oxygen bottles.

The particulate-nitrogen, ammonia-nitrogen, nitrite-nitrogen, nitrate-nitrogen, and dissolved oxygen of the first two bottles filled with subsample and the last two bottles were determined at once. These were used for the purpose of showing the initial concentration of the remaining oxygen bottles of subsamples. The remaining subsamples placed in separate dark rooms kept at 20°C and 30°C and covered with sheets of black polyethylen.

After the storage in the dark, individual four bottles of subsample in both temperatures of 30°C and 20°C were withdrawn at certain intervals and used for the determination of dissolved oxygen and different forms of nitrogen in duplicate. Analyses for nitrite and nitrate were made on filtered water that passed through a type HA Millipore (Millipore Filter Corp., Bedford, Mass.) with a 0.45-μ pore size, and analysis for particulate nitrogen was made on filtered water. Analysis for ammonia was made on unfiltered water. The subsamples collected in the experiment after darkening were frozen and stored until a convenient numbers had been collected for analysis with the exception of the sample of dissolved oxygen.

Dissolved oxygen was determined by the Winkler method described by THOMPSON and ROBINSON (1939). Ammonia was determined using Nessler's reagent improved by Winkler after distillation of ammonia in sample with strong alkali, in which there is an advantage to prevent the precipitation of calcium hydroxide and magnesium hydroxide formed by the addition of Nessler's reagent reacting with magnesium ion and calcium ion in sea water sample. Particulate-nitrogen was determined by a micro-Kjeldahl method. The particulate sample was digested for 3-4 hours with two m*l* concentrated sulfuric acid and 5 mg of catalyst mixtures prepared by grinding together potassium sulfate, cupric sulfate, and powdered selenium. After cooling, the digested sample is placed in 25-m*l* calibrated flask filled with ammonia-free water, and then the ammonium-nitrogen contained in the sample was determined by a steam-distillation method described above.

Nitrite-nitrogen was determined by the method of BENDSCHNEIDER and ROBINSON (1952), in which the nitrite was diazotized with sulphanilamide, and then coupled with N-(1-naphtyl)-ethylenediamine to produce a deep red colour. Nitrate-nitrogen was determined by the method of WOOD *et al.* (1967). The sample was treated with tetrasodium ethylenediamine tetraacetate solution and passed through a column of copperized cadmium fillings. By this treatment, nearly quantitive reduction of nitrate to nitrite resulted. The reduced nitrite-nitrogen was determined by the diazotization method described above. The nitrate-nitrogen value was obtained by subtracting nitrite-nitrogen in the water before the reduction.

3. Results and discussion

1. *Particulate-nitrogen*

The biochemical decomposition of particulate-nitrogen in stored sea water was commenced immediately after the storage in the dark at 30°C. During the first thirty days, about 75 per cent of the particulate-nitrogen present at the beginning of this experiment was decomposed in an exponential curve. From thirty to forty-four

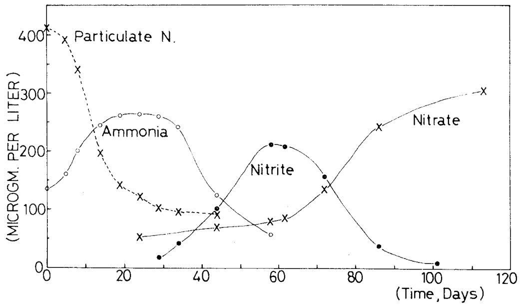

Fig. 1. The different forms of nitrogen produced by the biochemical decomposition and oxidation of the diatom *Sk. costatum* in the dark at 30°C.

Table 1. Concentrations of the dissolved oxygen and the different forms of nitrogen produced by the biochemical decomposition and oxidation of the diatom *Sk. costatum* in the dark at 30°C.

Time, days	Dissolved oxygen (m*l*/*l*)	NH_4-N (μg/*l*)	NO_2-N (μg/*l*)	NO_3-N (μg/*l*)	Particulate nitrogen (μg/*l*)
0	6.00	135	1.5	49.3	410
5	6.70	162	3.0	48.2	393
8	6.25	200	2.6	53.5	340
14	6.16	243	1.7	51.3	198
19	5.91	261	4.5	52.8	144
24	5.76	263	6.8	51.0	121
29	5.67	261	17.8	66.5	101
34	5.49	243	43.2	61.3	98
44	5.52	121	100.1	67.3	98
58	5.04	57	210.3	78.4	—
62	5.06	57	208.4	80.8	—
72	4.84	—	150.6	136.1	—
86	4.63	—	39.2	243.3	—
101	4.48	—	10.1	301.9	—
113	4.29	—	—	—	—

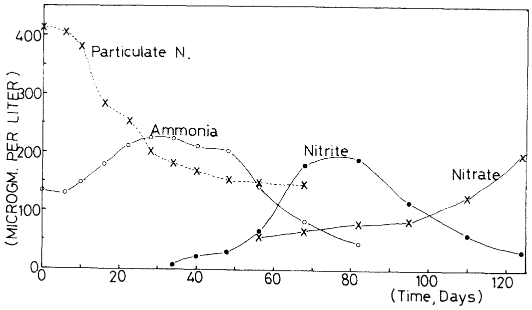

Fig. 2. The different forms of nitrogen produced by the biochemical decomposition and oxidation of the diatom *Sk. costatum* in the dark at 20°C.

Table 2. Concentrations of the dissolved oxygen and the different forms of nitrogen produced by the biochemical decomposition and oxidation of the diatom *Sk. costatum* in the dark at 20°C.

Time, days	Dissolved oxygen (ml/l)	NH_4-N (μg/l)	NO_2-N (μg/l)	NO_3-N (μg/l)	Particulate nitrogen (μg/l)
0	9.00	135	1.5	49.3	410
6	7.48	130	1.5	48.6	407
10	7.02	150	2.2	55.0	372
11	6.66	180	1.7	55.3	289
22	6.48	212	1.7	48.7	253
28	6.36	229	2.3	48.9	200
34	6.12	228	6.7	51.0	175
40	5.99	211	17.2	52.4	164
48	5.86	203	21.0	52.0	152
56	5.61	142	61.8	57.4	149
68	5.53	84	171.3	60.1	148
82	5.26	—	191.4	70.3	—
95	4.92	—	112.7	83.7	—
110	4.83	—	58.1	119.4	—
124	4.70	—	31.3	179.7	—

days, the biochemical decomposition of particulate-nitrogen was not almost observed as shown Fig. 1 and Table 1. At 20°C temperature, on the other hand, during the first thirty days only 50 per cent of the particulate-nitrogen was decomposed. Even on the first sixty-eight days after the storage, the biochemical decomposition of particulate-nitrogen was not more than 60 per cent (Fig. 2 and Table 2). Thus, rate and extent of the biochemical decomposition of particulate-nitrogen differ with each stored temperature. It is not confirmed whether their differences are due to differences in the bacterial flora of the water itself or in the water temperature which might influence the growth of bacteria, as described by VON BRAND *et al.* (1939) and WAKSMAN and CAREY (1935).

Furthermore, it seems from Figs. 1 and 2 (or Tables 1 and 2) that some parts of plankton constituting 30 to 40 per cent of the whole body is very resistant to further biochemical decomposition. According to Kamatani's observation (1968), some 70 to 80 per cent of the elementary nitrogen composition of plankton is more easily affected by biochemical decomposition and the residual fractions are hard to be affected by biochemical decomposition and oxidation. VON BRAND *et al.* (1937) pointed out also that under natural conditions in the sea the plankton is incompletely decomposed, and a large part of the particulate-nitrogen found in the deeper levels may be contained in such resistant or slowly decomposing plankton and bacterial residues.

2. *Ammonium-nitrogen*

As shown in Fig. 1 and Table 1, ammonia in the water appeared rapidly and simultaneously with the beginning of the biochemical decomposition of particulate-nitrogen in the sample after the storage in the dark at 30°C. When the biochemical decomposition of particulate-nitrogen approached almost to the end which occurred on the first twenty days after the system was darkened, ammonia reached a maximum concentration of ca. 263 μg per liter. The condition of its maximum was kept on for a period of about ten days. After this, it was becoming to disappear gradually with the conversion of ammonia into nitrite as time went on. The period from the appearance of ammonia to its disappearance was about sixty days.

Concerning the appearance of ammonia at 20°C, on the other hand, it is an interesting fact found in Fig. 2 and Table 2 that ammonia did not almost appear during the first ten days no matter when the biochemical decomposition of particulate-nitrogen was commenced immediately after the storage in the dark. After thirty days from the beginning of this experiment, the ammonia reached its maximum concentration of 229 μg per liter. After this, the ammonia began to disappear very slowly up to fifty day, and then disapperred rapidly as time went on. However, the period from the appearance of ammonia to its disappearance was longer than about thirty days as compared with that at 30°C.

Lastly, although the initial ammonia present at the beginning of this experiment which had been dispensed from the mother sample by a syphon already contained 135 μg per liter, it is not clear whether this excessively high concentration is because the mother sample was put aside for several days or because the sea water diluting the culture medium contained a remarkable amount of ammonia.

3. *Nitrite-nitrogen*

The appearance of nitrite began after the disappearance of ammonia at both temperatures of 20°C and 30°C, as shown in Figs. 1 and 2. Nitrite reaches its maximum when the ammonia approaches approximately to its maximum. The concentration of nitrite at the maximum amounts to ca. 210 μg at 30°C and ca. 190 μg at 20°C, per liter, respectively and both their concentrations correspond to the reduction of about 15 per cent of each maximum concentration of ammonia at both temperatures. These reduction may correspond to Spencer's observation (1956), where the failure of a sample of water to oxidize ammonia to nitrite has shown to be not due to the absence of catalytic bacteria in the water, but rather due to the lack of suitable nutrient conditions for the proliferation of the nitrifying bacteria. After the maximum of nitrite at 30°C it disappeared more rapidly with the process of time than at 20°C. However, the period from the maximum of nitrite to its disappearance required the same time as that from the appearance of nitrite to its maximum in either case. The total duration of the presence of nitrite was about sixty days at 30°C and about eighty days at 20°C respectively.

It is found from Figs. 1 and 2 that the time lag in the oxidation of ammonia to nitrite at 20°C and 30°C temperature is recognized clearly in the present experiment. VON BRAND *et al.* (1939) pointed out that the time lag in the said oxidation is apparently not due to the absence of the necessary bacteria, but rather it may in some way relate to the continuous aeration. However, there is a doubt whether the observation by VON BRAND *et al.* (1939) right or not. Because in the present experiment the dissolved oxygen content remains more than sufficient for the biochemical oxidation of nitrogenous organic matter in the sample. After all, the time lag in the oxidation of ammonia to nitrite and finally to nitrate appears to be caused by the bacterial activity relating to temperature.

From the above results it is found that the total duration of the appearance of nitrite differs with temperature, and the time taken for the maximum of nitrite after the system was darkened is a time lag of about ten days between 20°C and 30°C. The appearance of nitrite begins after the maximum of ammonia, and the maximum concentration of nitrite appears when the ammonia disappears completely.

4. *Nitrate-nitrogen*

Nitrate at both temperatures of 30°C and 20°C began to appear immediately after nitrite reached each maximum concentration, and then increased slowly in the water as time went on, as shown in Figs. 1 and 2. This result corresponds almost precisely to the observation by VON BRAND *et al.*, where the nitrate begins to appear only when the nitrite disappears, and this never seems to happen so long as a significant amount of ammonia remains. However, the maximum of nitrate seems to have no connexion with the minimum of nitrite, although the ammonia reaches the maximum concentration when the biochemical decomposition of particulate-nitrogen in sea water approaches almost to the end and the nitrite reaches the maximum concentration when ammonia reaches the minimum as already described.

It is necessary to state here that biochemical decompositon and regeneration of nitrogenous organic matter in sea water had been also investigated experimentally by VON BRAND *et al.* (1939), GRILL and RICHARDS (1963), and and KAMATANI (1968) under the high concentration of nitrogenous organic matter as compared with that of the present experiment. These same authors' observations correspond almost to the present one.

5. *Oxygen consumption*

The change of oxygen consumption accompanying the biochemical oxidation of nitrogenous organic matter at both temperatures of 20°C and 30°C is shown in Fig. 3. The rate of oxygen

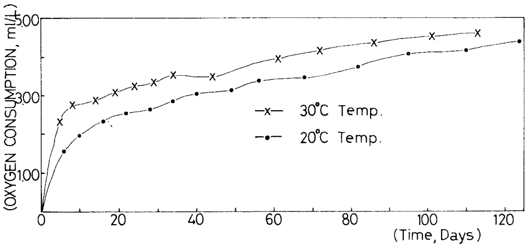

Fig. 3. Oxygen consumption accompanying the biochemical decomposition and oxidation of the diatom *Sk. costatum* in the dark at both temperatures of 20°C and 30°C.

consumption is promoted with increasing temperature, and the extent of it increases exponentially during the first twenty days at 30°C and/or during the first thirty days at 20°C, respectively. After this, the oxygen consumption at both temperatures increases gradually in linear curve until the end of each experiment. The total amount of oxygen consumption is nearly 4.50 ml per liter at both temperatures, although the periods of both experiments after the system was darkened differ. The further detailed description of oxygen consumption is omitted here, because rate and extent of oxygen consumption are influenced by the relative amount of oxygen-consuming organic matter to the dissolved oxygen content in sea water as in other reports by the present authors (1969a and '69b).

An interesting fact found from Fig. 3 is that the period of oxygen consumption is subdivided into two phases; that is, an exponential phase and a linear phase. The time shifting from an exponential phase to a linear phase corresponds just to the maximum concentration of ammonia or the end of the biochemical decomposition of particulate-nitrogen. After all, it may be implied that during the exponential phase the oxygen consumption is caused largely by the respiration accompanying the increase of bacterial population as in the report by WAKSMAN and CAREY (1935), where the rapid oxygen consumption during the first decomposing stage of organic matter is due to the proliferation of planktonic bacteria. Concerning the oxygen consumption at the linear phase on the other hand it may be implied that the biota in a sample is becoming essentially constant, from the point of veiw that the extent of oxygen consumption is considerably little no matter when the residual dissolved oxygen exists more than sufficient in subsample of oxygen bottles. Namely, it is assumed that the oxygen consumption during the linear phase is almost used for the biochemical oxidation of ammonia to nitrite and finally to nitrate. This detailed discussion will be described later.

6. *Different forms of nitrogen-oxygen consumption relation*

The plot of the different forms of nitrogen which appeared in biochemical decomposition and regeneration of nitrogenous organic matter or disappeared in the biochemical oxidation of its decomposition products to the oxygen consumption at both temperatures of 30°C and 20°C is shown in Figs. 4 and 5, respectively. The solid lines show the correlation between oxygen con-

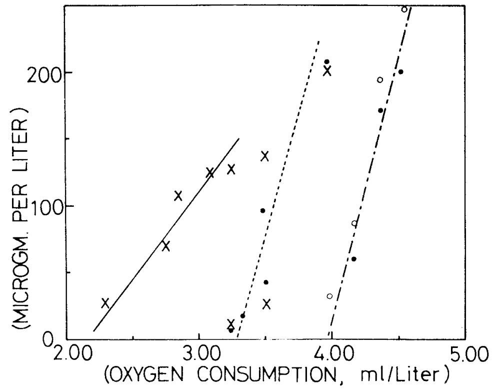

Fig. 4. Relation between the oxygen consumption and the different forms of nitrogen at 30°C. Solid line indicates the correlation between the oxygen consumption and the ammonia (×) appeared by the biochemical decomposition of particulate-nitrogen. Dotted line indicates the correlation between the oxygen consumption and the nitrite (●) appeared by the biochemical oxidation of ammonia (simultaneously plots the concentration of ammonia (×) disappeared by the biochemical oxidation of ammonia to nitrite). Dashed line indicates the correlation between the oxygen consumption and the nitrate (○) appeared by the biochemical oxidation of nitrite (simultaneously plots the concentration of nitrite (●) disappeared by the biochemical oxidation of nitrite to nitrate). The concentration of oxygen consumption is computed from the initial dissolved oxygen at the beginning experiment.

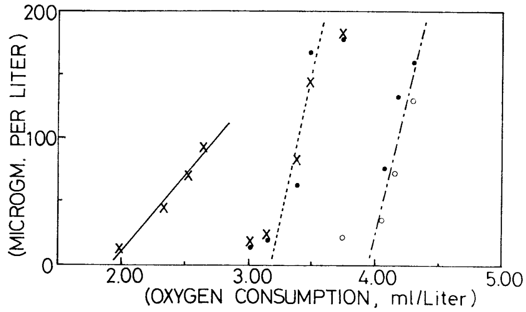

Fig. 5. Relation between the oxygen consumption and the different forms of nitrogen at 20°C. Various signs are precisely the same one in Fig. 4.

sumption and appearance of ammonium-nitrogen caused by the biochemical decomposition of particulate-nitrogen. The dotted lines show the correlation between oxygen consumption and nitrite-nitrogen appeared in the biochemical oxidation of ammonia (simultaneously plot the concentration of ammonia which disappeared in the biochemical oxidation of ammonium-nitrogen to nitrite-nitrogen). The dashed lines show the correlation between oxygen consumption and nitrite-nitrogen which appeared in the biochemical oxidation of nitrate (simultaneously plot the concentration of nitrite which disappeared in the biochemical oxidation of nitrite-nitrogen to nitrate-nitrogen).

Between oxygen consumption and ammonia-N, nitrite-N, and nitrate-N produced by biochemical decomposition and oxidation of nitrogenous organic matter there is a fair correlation, which is linear as shown in Figs. 4 and 5. Its linear correlation may imply that the ratio of oxygen consumption to the appearance of one atom of ammonia-N, nitrite-N, and nitrate-N is constant at various stages of biochemical decomposition and oxidation of nitogenous organic matter and has no relation to temperature and/or period of experiment. In addition, the gradient of the dashed line and that of dotted line indicate approximately the same inclination. It may be inferred from above facts that the biochemical oxidation of ammonia to nitrite and finally to nitrate accompanies a certain constant consumption of the dissolved oxygen, while the rate of regeneration of the different forms of nitrogen and the rate of oxygen consumption indicate somewhat a time lag. On the other hand, the ratio of the oxygen consumption to the appearance of ammonia caused by the biochemical decomposition of particulate-nitrogen (solid lines in Figs. 4 and 5) is higher as compared with that of other forms of nitrogen. It may be explained by the oxygen consumption required for the oxidation of organic carbon in the respiration accompanying the increment of bacterial population at the first decomposing process of organic matter as described in the first decomposing process of organic matter as described in the report ZOBELL and ANDERSON (1936a), where there was found a much greater increase in numbers of bacteria at the early decomposition stage when water was stored in small bottles than in large bottles.

Finally, as concluding remark, it seems that the present experimental results can be applied for nitrogen cycle and oxygen consumption accompanying the biochemical oxidation of nitrogenous organic matter in the ocean. Because, in general, it is known from ZoBell and Anderson's observation (1936b) that greatest numbers of marine bacteria have been found in the coastal sea and in the euphotic zone of open ocean, but this phenomenon is not almost observed below the euphotic zone. It may be thereby considered that the oxidation of ammonia to nitrite and finally to nitrate will proceeds while certain constant ratios for the oxygen consumption are kept, regardless of depth below the euphotic zone in the open ocean. In fact, REDFIELD (1934) pointed out statistically that the correlation between concentration of nitrate and amount of oxygen utilized in waters of Western Atlantic Ocean indicates a linear.

References

BENDSCHNEIDER, K. and R. J. ROBINSON (1952): A new spectrophotometric determination of nitrite in sea water. Jour. Mar. Res., 11, 87-96.

VON BRAND, T., N. W. RAKESTRAW and C. E. RENN (1937): The experimental decomposition and regeneration of nitrogenous organic matter in sea water. Biol. Bull., **72**, 165-175.

VON BRAND, T., N. W. RAKESTRAW and C. E. RENN (1939): Further experiments on the decomposition and regeneration of nitrogeneous organic matter in sea water. Biol. Bull., **77**, 285-296.

VON BRAND, T. and N. W. RAKESTRAW (1940-42): Decomposition and regeneration of nitrogenous organic matter in sea water. III-V. Biol. Bull., 79, 81, and 82.

COOPER, L. H. N. (1936): The nitrogen cycle in sea water. Jour. Mar. Biol. Ass., **22**, 183-204.

GRILL, E. W. and F. A. RICHARDS (1963): Nutrient regeneration from phytoplankton decomposing in sea water. Jour. Mar. Res., **22**, 51-69.

HARRIS, E. (1959): The nitrogen cycle in Long Island Sound. Bull. Bingham Oceanogr. Coll., **17**, 31-65.

HAMILTON, R. D. (1964): Photochemical processes in the inorganic nitrogen cycle of the sea. Lim nol. Oceanogr,. **9**, 107-111.

KAMATANI, A. (1968): A study on the regeneration of inorganic nutrient from diatom decomposition in the ocean. Doctor Thesis. Tohoku University.

MOTOHASHI, K. and C. MATSUDAIRA (1969a): On the oxygen consumption accompanying the decomposition of diatom.—Its relation to diatom population—Tohoku Jour. Agr. Res., **20**, 73-80.

MOTOHASHI, K. and C. MATSUDAIRA (1969b): Some problems relating to phosphate regeneration and oxygen consumption in sea water.—Phosphate regenerated by zooplankton during excessive grazing—Tohoku Jour. Agr. Res., **20**, 81-88.

MOTOHASHI, K. and C. MATSUDAIRA (1969c): On the relation between the oxygen consumption and the phosphate regeneration from phytoplankton decomposing in stored sea water. Jour. Oceanogr. Soc. Japan, **25**(5), 249-254.

REDFIELD, A. C. (1934): On the proportions of organic derivatives in sea water and their relation to the decomposition of plankton. In: James Johnstone Memorial Volume. Univ. Liverpool Press.

SPENCER, C. P. (1956): The bacterial oxidation of ammonia in the sea. Jour. Mar. Biol. Ass., **35**, 621-630.

THOMPSON, T. G. and R. ROBINSON (1939): Notes on the determination of dissolved oxygen in sea water. Jour. Mar. Res., **2**, 1-8.

VACCARO, R. F. (1963): Available nitrogen and the biochemical cycle in the Atlantic off New England. Jour. Mar. Res., **21**, 284-301.

VACCARO, R. F. and J. H. RYTHER (1960): Marine phytoplankton and the distribution of nitrite in the sea. Jour. du Conseil, **25**, 260-271.

WAKSMAN, S. A. and C. L. CAREY (1935): Decomposition of organic matter in sea water by bacteria. Jour. Bact., **29**, 531-543.

WOOD, E. D., F. A. J. ARMSTRONG and F. A. RICHARDS (1967): Determination of nitrate in sea water by cadmium-copper reduction to nitrite. Jour. Mar. Biol. Ass., **47**, 23-31,

ZOBELL, C. E. and D. Q. ANDERSON (1936a): Observation on the multiplication of bacteria in different volumes of stored sea water and influence of oxygen tension and solid surface. Biol. Bull., **71**, 324-342.

ZOBELL, C. E. and D. Q. ANDERSON (1936b): Vertical distribution of bacteria in marine sediments. Bull. Amer. Ass. Petrol. Geol., **20**, 260.

海水における窒素化合物の生化学的分解・酸化に伴う酸素消費について

本橋敬之助　松平近義

要旨: 窒素化合物として珪藻プランクトン(*Sk. costatum*)を20°C, 30°Cの暗所に保存し，その分解・酸化に伴う酸素消費を研究した。珪藻体の分解は暗所保存直後に起りアンモニアを放出した。アンモニア・亜硝酸・硝酸の各段階における酸化過程は20°Cと30°Cの間に明瞭な時間的差異があった。珪藻プランクトンの分解・酸化に伴う酸素消費は対数期と直線期の二段階に区分され，その段階遷移期はアンモニア最大出現期あるいは珪藻体の分解終期に相当していた。更に，放出したアンモニア・亜硝酸・硝酸と酸素消費の間には直線相関が見られ，外海の受光層以深ではアンモニアから亜硝酸・硝酸への酸化にはある一定の比率の酸素が消費されることを実験的に確めた。

La mer (Bulletin de la Société franco-japonaise d'océanographie)
Tome 7, N° 4, Novembre 1969

An Energy Consideration on the Formation of Foam in Sea Water*

—The Production of a Bubble by Falling Drop Method and its Energy Consideration—

Tomosaburo ABE** and Nobuo MORITANI**

Abstract: When the rain drop falls onto the water surface, a bubble, sometimes, is formed on there on; whence, we try to have a drop of sea water, generated at the tip of a nozzle and fallen slowly onto the water surface of the tank filled with sea water. From this experiment, it is found that a bubble is produced when the following conditions are satisfied.

(1) The height H from the tip of a nozzle to the surface of sea water must be held a discrete value.

(2) The mass of a drop M must be larger than a certain value.

The above mentioned results are found to be related mainly to the oscillation of the falling drop and to the energy which the drop holds when it contacts with the surface of the sea water. Next, in order to demonstrate the successive stages of growing bubble and jet —a jet spurts when a bubble is not produced—photographs are taken, whence surface and potential energies of bubble and those of jet are calculated using these photographs.

1. Introduction

Recently more interest has been taken in the problem on bubble and foam of sea water, and many studies have been reported concerning decay of sea foam, its stability, stable foam, damages due to stable masses of foam transported inland by strong winds, the relation between droplets which come from the decaying of sea foam and salt nuclei in atmosphere which are considered to be produced through the bursting process of the bubbles on sea surface, and slicks, etc.

Then, in order to consider the mechanism and feature of the formation of foam and bubble in the open sea and ashore, an experiment of the production of a bubble with falling drop using techniques of electronics is done as the fundamental studies. The present paper is a report of them.

2. Apparatus and experimental procedures

The schematic diagram of the apparatus, which is used to for the production of a bubble by the falling drop method, is shown in Fig. 1. This apparatus is set in a box, whose front is made of a sheet of glass, in order to shut out the dust and to keep the inside of the box at a constant temperature. In Fig. 1, T_U is the upper tank and T_L lower tank and in these tanks are contained the same quantity of sea water, respectively. The sea water in tank T_L and that in tank T_0 installed outside the box, can circulate into each other as shown in the Fig. 1. Then, when the cock C is opened the water in the tank T_0 flows into the tank T_L, and then the sea water in tank T_L overfows into another tank T_A installed around T_L and as a result of this procedures the surface of the sea water in tank T_L is cleaned.

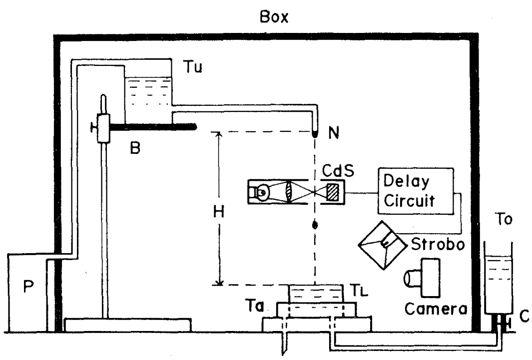

Fig. 1. Schematic diagram of the apparatus.

A drop is made at the tip of the nozzle N by pushing the pump P and then it falls onto the surface of the sea water in tank T_L. The

* Received August 2, 1969

** Department of Physics, Science University of Tokyo

height H of the tip of the nozzle over the surface of the sea water in tank T_L is changeable by setting the tank T_U on the base B which is movable vertically, and a drop, therefore, is able to fall from various heights.

In case, the photographs of growing stages of bubble and jet are taken, we make use of lamp, lens, CdS (photoconductor), delaying circuit, stroboscopic apparatus and camera, as described in the following. First. as the light of the lamp converges on the front part of the CdS through the lens forehand, a pulse occurs at the instant when the drop from the nozzle is passing by along the front part of the CdS and shuts out the light. Next, the sign of the pulse is delayed suitably by the work of delaying circuit and this delayed sign of the pulse works on the stroboscopic apparatus. In this way the photographs can be taken rather easily to catch all the growing stages of bubble and jet.

Diameter of the nozzle and mass of a drop

The nozzles N used in this experiment are made of acrylite. The section of the nozzle is shown in Fig. 2. As the nozzle is changeable, we can vary the mass M of the falling drop from the nozzle by means of changing the diameter D of the nozzle. The relation between the mass M of the drop and the diameter D of the nozzle is shown Fig. 3 and Table 1. From Fig. 3 it follows that M is propotional to D on the condition that the value of D is smaller than 9.5 mm. Therefore, in the following experiment nozzles having diameters 5.0 to 9.5 mm are used. From Table 1 it is observed that the fluctuation of each M produced by the nozzle having the same diameter is fairly small. Next, the relation between the temperature θ and the mass M of the drop which falls from the nozzle—the diameter of the nozzle is 8.0 mm (Nozzle number VII)—is shown in Fig. 4. From the Fig. 4 it is found that the change in mass M is of considerable value for the moderate change of temperature θ. The drop, therefore, must be kept at a constant temperature as possible, throughout the whole stages of the experiment.

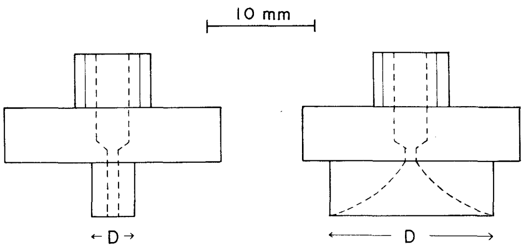

Fig. 2. The sections of nozzles.
Nozzle number I~IV. Nozzle number V~X.

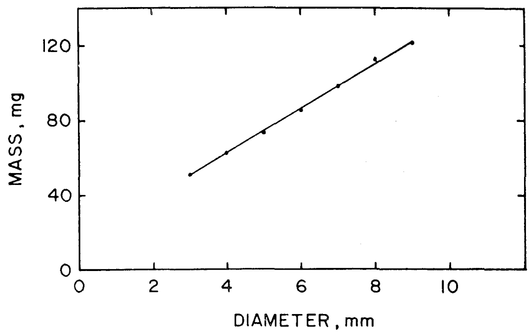

Fig. 3. Relation between M and D.

Table 1. The diameter of nozzle and the mass of drop.

Diameter (No.)	Case of experiment 1	2	3	Mean value	Deviation
mm	mg	mg	mg	mg	mg
3.0 (I)	51.5	50.5	51.0	51.0	± 0.5
4.0 (III)	62.0	63.0	62.0	62.3	± 0.7
5.0 (V)	73.0	74.5	73.0	73.5	± 1.0
6.0 (VI)	85.5	85.5	86.0	85.7	± 0.3
7.0 (VII)	98.0	99.0	97.0	98.0	± 1.0
8.0 (VIII)	110.0	113.0	112.5	111.9	± 1.1
9.0 (IX)	121.0	121.0	122.0	121.3	+ 0.7
9.5 (X)	113.5	112.0	129.0	118.0	±11.0

Note: (No.): Nozzle number
Sea water temperature: 20~22°C

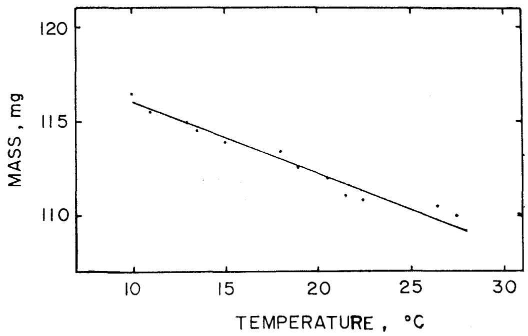

Fig. 4. Relation between M and θ.

Note: The diameter of nozzle is 8.0 mm (No. VII)

3. Results and discussions

A drop of the sea water made at the tip of the nozzle falls onto the surface of the sea water in the the tank T_L from every conceivable height H which is the distance from the tip of a nozzle to the surface of the sea water and produces a bubble, whose life time is always less than 1 second, on the sea water surface at the definite height. The relation between height H_n ($n=2$, 3, 4) where a bubble is produced and each mass of drop M, and the provability of the production of a bubble at the height H_n, are shown in Table 2 and Fig. 5. On examining these data, following results are obtained.

(1) A bubble is produced at the discrete values of the height (That is; at $H_n=H_2$, H_3, H_4) angainst each mass M of drops.

(2) The value of the height H_n becomes larger in proportion to the mass M of the drop.

(3) The heigher the H_n grows, the wider tends to become the range where a bubble is produced.

(4) When the value of M is smaller than 60 mg, it becomes more difficult for the drop to produce a bubble. When the value is 50 mg, the bubble is not produced at any height.

(5) The heigher H_n grows, the more difficult tends to become to produce a bubble, and at the height where H is more than H_4 a bubble is seldom produced.

Hence, in order to take these interesting results into consideration stroboscopic photographs of a falling drop are taken (Fig. 6). From the Fig. 6 it is found that the falling drop is remarkably oscillating about its own spherical form and a bubble is produced only when the drop has a vertically long ellipsoidal shape at the instant when it contacts with the surface. Considering such a fact, the results (1), (2) and (3) will

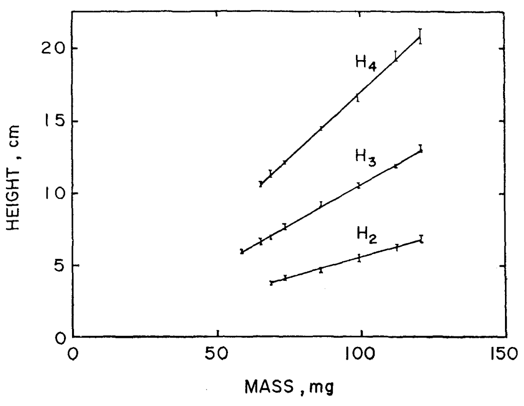

Fig. 5. Relation between H and M.

Note: H_2, H_3 and H_4 are the discrete height at which a bubble is produced.

Table 2. Results of the experiment.

M (mg)	H_n	H cm	P (%)
52.7	H_2	—	—
	H_3	—	—
	H_4	—	—
58.3	H_2	—	—
	H_3	5.70	20
		5.85	100
		6.00	100
	H_4	—	—
64.3	H_2	—	—
	H_3	6.00	20
		6.15	100
		6.30	60
		6.45	20
	H_4	10.35	40
		10.50	0
		10.65	20
76.8	H_2	3.60	100
	H_3	6.60	80
		6.75	40
	H_4	10.95	60
		11.10	80
		11.25	40
73.5	H_2	3.90	40
		4.05	100
		4.20	20
	H_3	7.50	100
		7.65	100
		7.85	40
	H_4	12.00	20
		12.15	30
86.1	H_2	4.50	70
		4.65	100
		4.80	80
	H_3	9.00	100
		9.15	50
		9.30	20

M (mg)	H_n	H cm	P (%)
86.1	H_4	14.40	40
		14.55	40
99.2	H_2	5.25	100
		5.40	100
		5.55	100
		5.70	20
	H_3	10.35	10
		10.50	80
		10.65	50
	H_4	16.35	30
		16.50	80
		16.65	100
		16.80	100
		16.95	40
112.6	H_2	6.00	80
		6.15	100
		6.30	100
		6.45	40
	H_3	11.85	20
		12.00	30
	H_4	19.20	20
		19.35	40
		19.50	100
		19.65	80
		19.80	20
121.5	H_2	6.60	100
		6.75	100
		6.90	100
		7.05	20
	H_3	12.90	30
		13.05	70
		13.20	50
		13.35	30
	H_4	20.25	30
		20.40	60
		20.55	100
		20.70	40
		20.85	40
		21.00	40
		21.15	60
		21.30	60

Note: Sea water temperature 20~22°C
Where H_n is the height and P is the probability when a drop produces a bubble.

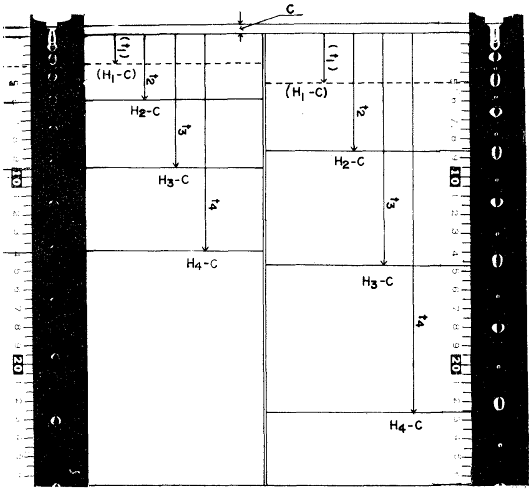

$\omega=3.00\times10^3$ c/sec $\quad$ $\omega=2.66\times10^3$ c/sec

$M=73.5$ mg $\quad$ $M=121$ mg

Fig. 6. The feature of a falling drop by stroboscopic method.

Note: ω: frequency of stroboscope
M: mass of drop.

be explained easily. At the heights H_1, where the drop takes a vertically long ellipsoidal form, however, a bubble is not produced (see Fig. 6). It seems that the potential energy of the drop which falls from the height H_1 is too small for the drop to break into the surface of sea water and to produce a bubble. The result (4) is to be explained as described in the following. When the mass of a drop M is smaller than a certain value—that is; its volume becomes much smaller—the influence of the surface tension of the drop is so marked that the drop cannot oscillate to great degree about the spherical form, and the damping of the oscillation will be increased. Then the falling drop cannot take the favorable form for the bubble production—that is, a vertically long ellipsoidal form. Moreover, it will be caused by another reason that the potential energy of the drop is too small for the drop to produce a bubble. The result of (5)—that is; it becomes more difficult to prcduce a bubble at the heigher position—may be partly caused by the damping of the falling drop.

4. Consideration of the relation between H_n and M

The relation between H_n and M is to be discussed in consideration of the fact that a falling drop oscillates. The frequency and descending distance of an oscillating drop are expressed by the following equations neglecting the resistance of the air;

$$\omega^2=\frac{8T}{3\pi M}, \tag{1}$$

$$H-C=\frac{1}{2}gt^2, \tag{2}$$

where ω: frequency of drop
T: surface tention of drop
g: acceleration of gravity
H: the height from the surface of sea water to the tip of nozzle
$H-C$: the height from the surface of sea water to the center of a drop which is hanging at the tip of a nozzle.

(The value of C is assumed to be constant for brevity, though it will be slightly variable according to M.)

Considering that the hanging drop takes a vertically long shape, the duration time t_n which takes the hanging drop arrives at the distance of H_n, is

$$t_n=\frac{n}{\omega}, \tag{3}$$

where $n=2$, 3, 4 mean the oscillation numbers. Because the shape of the drop is also vertically long at the height H_n.

Therefore, upon substituting H for H_n, we have from (1), (2) and (3)

$$H_n-C=K_nM, \tag{4}$$

where $K_n=\frac{3\pi g}{16T}n^2$.

From the equation (4), it is found that H_n-C is proportional to M, on the condition that n and T are constant. In Fig. 7 the theoretical curve of height H *versus* mass M derived from the equation (4) and that obtained from the present experiments are shown. The latter curve is much steeper than the former, although both curves are expected to agree well with each other. This main reason will be caused by the fact that the frequency of the drop, in the first, second and third cycles, is considerably smaller than the theoretical value given by the equation (1) (see Table 3). Because the drop hanging at the tip of a nozzle would suffer the adherent

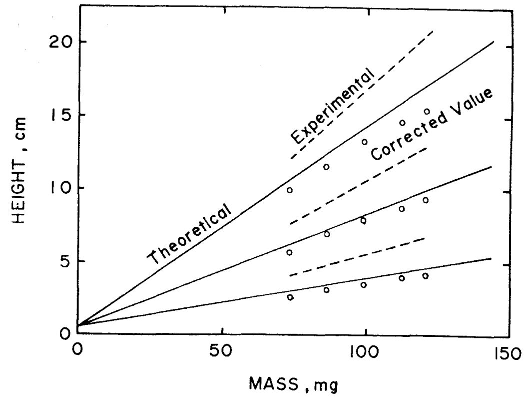

Fig. 7. Comparison between theoretical and experimental values.

Table 3. The frequency of drop.

ω (c/sec)	Mass M of drop (mg)				
	73.5	86.1	99.2	112.6	121.5
ω_{02}	23.5	21.7	20.0	18.6	17.7
ω_{23}	26.1	23.7	21.9	20.5	19.7
ω_{34}	27.5	25.2	23.6	21.4	20.6
ω_0	27.8	25.7	23.9	22.5	21.6

Note;

ω: the frequency of drop

ω_{02}: the mean value of the frequency of drop between $H=0$ and $H=H_2$

ω_{23}: the mean value of the frequency of drop between H_2 and H_3

ω_{34}: the mean value of the frequency of drop between H_3 and H_4

ω_0: the frequency of drop obtained from equation (1).

effect of the surface of nozzle tip. And the value which is derived from the experiment is corrected considering the decreasing of the frequency, and their resultant values of this correction are shown in Fig. 7, with the circular marks.

5. The stages of bubble growing

The successive stages of the bubble growing are photographed in a special way mentioned above. As it is very difficult to take photographs of the stages of the bubble growing with exceedingly short interval—that is; a few mili second—concernig to the same drop. So we fall a number of drops and take the photographs by putting off the time length little by little for each drop making use of above-mentioned delaying curcuit and then grouping these obtained photographs, we imagined the stages of the bubble growing. These photographs are shown in Fig. 8. From the Fig. 8, the stages of the bubble growing are observed as following. First, a drop of sea water has the vertically long ellipsoidal form, in arriving at the water surface (1). As the drop falls into the sea water together with its neighboring water, a cavity is made in the subsurface (2). The cavity expands like the shape of a head of overturned mushroom (3, 4) and then, it separates into two parts and the separated cap turns into a bubble (5). While the bubble is descending, its shape is slightly extended to the vertically long direction (6, 7, 8). Then the bubble arrives at the surface of sea water (9) and at last it becomes a stable bubble within 200 msec (10).

Next, the energy of the bubble is calculated on the each stage using Fig. 8, as shown in Fig. 10-a—that is; the potential energy is calculated from shape and location of upper and lower parts of the water surface, and the surface energy is generated from the surface area of these parts. From the Fig. 10-a, it is found that the surface energy E_s of the bubble after 16 msec is nearly constant and on the contrary, the potential energy E_p of the bubble decreases after about 50 msec.

6. Comparision between the stages of bubble growing with those of jet growing

When a drop falls into the surface of the sea water, sometimes, a bubble is not produced but a jet spurts, in spite of H equal to H_n. Whence the successive stages of jet are taken by photographs as those cases of bubble (Fig. 9). Comparing Fig. 9 with Fig. 8, it is found that the most marked difference in the shape between the stages of bubble growing and those of jet growing occurrs at the time of 24 msec. That is; in the former stages the cavity in a subsurface separates into two parts at that time and on the contrary, in the latter stages neither it sparates nor has constriction. The change of the energy of jet is shown in Fig. 10-b. Then, from the Fig. 10-a and the Fig. 10-b, it is found that the surface energy of bubble is nearly

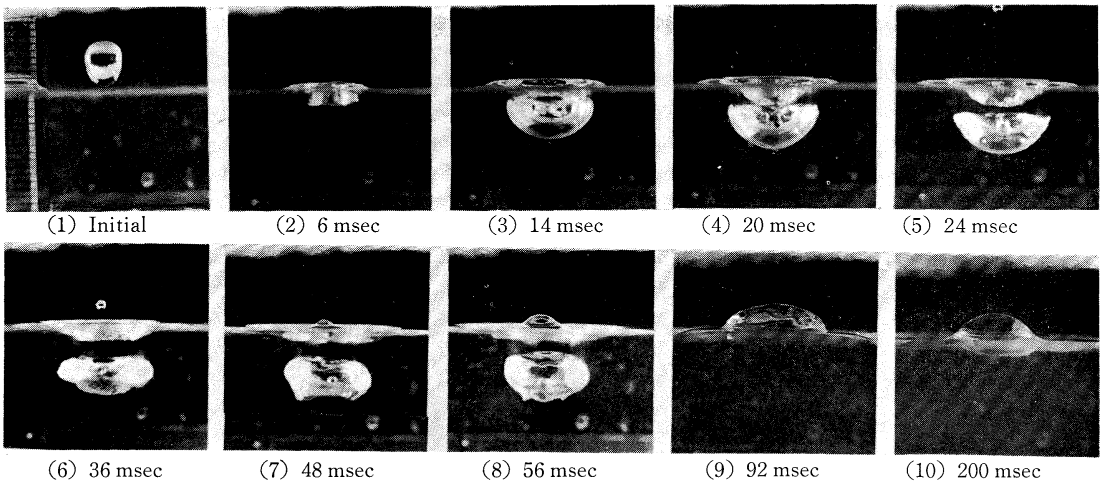

Fig. 8. The successive stages of the growing bubble. (M=98.0 mg, H=10.0 cm)

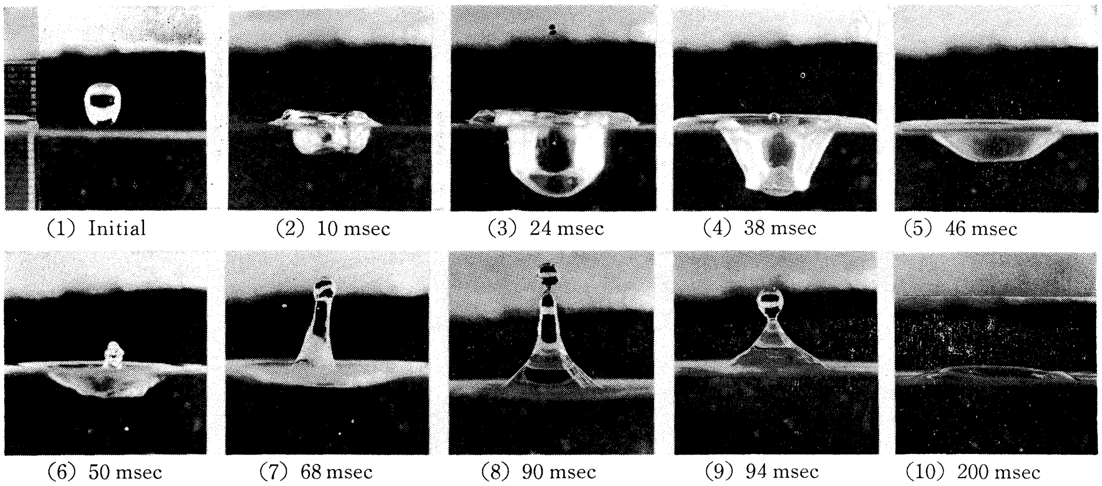

Fig. 9. The successive stages of the growing jet. (M=98.0 mg, H=10.0 cm)

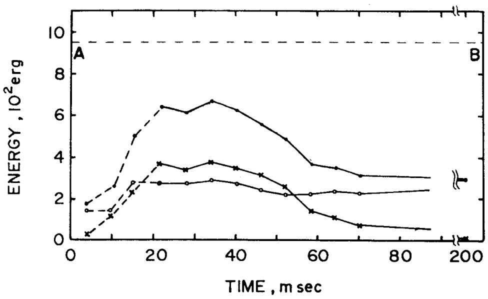

Fig. 10-a. The change of the energy "case of bubble".

Note: Dotted line A—B is shown the energy of a falling drop hold initially.

○—○ Surface energy of bubble (E_s)

×—× Potential energy of bubble (E_p)

●—● Total energy of bubble ($E=E_s+E_p$)

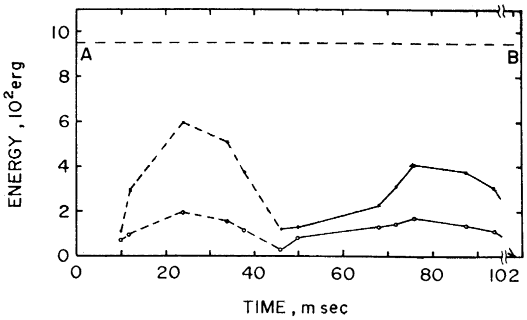

Fig. 10-b. The change of the energy "case of jet."

Note: Dotted line A—B is shown the energy of a falling drop hold initially.

○—○ Surface energy of jet (E_s)

●—● Total energy of jet ($E=E_s+E_p$)

constant after 16 msec and on the contrary that of jet is considerably changeable, and the total energy of jet is also more changeable than that of bubble. It means that the sea water is violently agitated with a falling drop when a jet is produced and on the other hand, when a bubble is produced, this agitation may be soften by the bubble. The qualitative consideration on the above interesting phenomenon will be discussed later.

Acknowledgements

The authors wish to express their sincere thanks to Mr. N. FUKUCHI of our laboratory, Science University of Tokyo, for his valuable information, to Messrs. S. SHIKE, G. KASAI, who are graduates of this University, to Messrs. N. FUKUDA, S. IWASAWA and others of our laboratory, who are now students of the University, for their helps throughout this research. Also, thanks are due to Mr. T. HASEGAWA who was a collaborator of N. MORITANI, one of the present authors, on the preliminary study experiment of this research which was graduate thesis of them.

References

1. ABE, T, (1953): A study on the foaming of sea water, on the mechanism of the decay of foam layer of sea water. Rec. Oceanogr. Wrks. Japan, **1**, no. 2, n.s. 18～24.
2. ABE, T. (1955): A study on the foaming of sea water. on the mechanism of the decay of bubbles and their distribution in foam layer of sea water. Pap. Met. Geophys., **5**, 240～247.
3. ABE, T. (1955): A study on the foaming of sea water, —tentative analysis of wind wave data in view of sea water—, *ibid*, **6**, 164～171.
4. ABE, T. (1962): On the stable foam formation of sea water in sea (preliminary report), Jour. Oceanogr. Soc. Japan 20th Ann. Vol., 242～250.
5. ABE, T. (1963): In situ formation of stable foam in sea water to cause salty wind damage, Pap. Met. Geophys., **14**, 93～108.
6. BIKERMAN, J. J. (1958): Surface Chemistry. Academic Press Inc., p. 501.
7. FRUEL, B. B. and W. D. HARKINS (1929): The shapes of drops. and the determination of surface tention. Jour. Phys. Chem., **33**, 1217～1234.
8. LAMB, H. (1932): Hydrodynamics. Cambridge Univ. Press. p. 738.

海水泡沫の生成に関するエネルギー論的考察

—海水滴落下による気泡の生成とそのエネルギー論的考察—

阿部友三郎　森谷誠生

要旨: 凝結核発生，塩害の問題等に関連して，最近海水の気泡と泡沫に関する諸問題が興味を持って研究されて来た。海洋における泡沫の崩壊，その安定度，安定泡沫，強風によって沿岸に吹き上げられた海水泡沫塊による塩害，海水表面に生じた気泡の崩壊過程で生成されると考えられる大気中の海塩微粒子，スリック等の研究が発表されてきた。この海洋に生成する泡沫の生成過程は複雑ではあるが，風等による海水の攪乱と密接な関係にあることは予想されよう。大きく動揺する海水は，そのエネルギーの一部を失って泡沫を生成する。この海水の動揺と，生じた泡沫との間の関係を考察するための基礎的研究として，海水滴落下による気泡生成の実験を行なった。

この実験により以下の結果が得られた。

（1） 海水滴から海水面までの高さが段階的な値のとき。

（2） 海水滴の質量がある値より大きいとき。

以上 (1), (2) の条件が満たされたときにのみ，この落下してきた海水滴によって気泡が生成した。そしてこの結果は，海水滴が落下中振動しており，海水面に突入するときの形状と，その海水滴が持っているエネルギーに関係していることがわかった。

次に，この気泡生成過程と，気泡が生成されずジェットが飛び出す事も有るので，このジェットの生成過程を，その実態を特殊写真撮影し，両者を比較対照しながら若干のエネルギー論的考察を行なった。

La mer (Bulletin de la Société franco-japonaise d'océanographie)
Tome 7, N° 4, Novembre 1969

Aerodynamic Roughness of the Sea Surface*

Noriyuki IWATA**

Abstract: In the turbulent boundary layer over a rigid surface having arbitrary roughness elements, it is found that the equivalent roughness length referred to Nikuradse's uniform sand-grain is proportional to the mean square slope of the surface considered of arbitrary roughness pattern.

Applying the same reasoning to the sea surface, we have found empirically that the roughness parameter u_*z_0/ν depends not only on u_*H/ν but also on the mean square slope of the sea surface. Assuming that the major part of the mean square slope of the sea surface could be ascribed to the equilibrium range of the power spectrum, it is concluded that the shear parameter of the wind gz_0/u_*^2 is not constant but changes with both $u_*^3/g\nu$ and gH/u_*^2 and that the drag coefficient is dependent not only on the mean wind velocity but also on the mean wave height caused by local wind.

Notation

H_s: average height of uniform sand-grain roughness of Nikuradse's experiments or equivalent roughness of arbitrary surface
ν: kinematic viscosity of the air
u_*: friction velocity, square root of surface stress divided by the density of the air
δ: thickness of viscous sublayer
U: mean velocity of the wind at arbitrary height in the turbulent boundary layer
H: average height of arbitrary roughness or of wave elevations of the sea surface
$\boldsymbol{\kappa}$: vector form of wave number
$\bar{s^2}$: mean square slope of arbitrary roughness elements or sea surface
σ: angular frequency of surface wave movement
T_0: mean value of zero-up crossing periods
T_p: mean value of crest-to-crest periods
L: average wave length of roughness elements or sea waves caused by local wind
ρ_w: density of sea water
T: surface tension of the sea surface

1. Introduction

Turbulent flow over a rigid surface is described as aerodynamically smooth or rough in the two limiting cases. In aerodynamically smooth flow, there is a viscous sublayer near the wall. In this region of the flow, the turbulent Reynolds stress is negligible and the constant total stress is supported by molecular viscosity. At the othe extreme, the surface is so rough that the wall stress is supported by the form drag of roughness elements of the surface.

In the air flow over the sea, where few or no ripples are present, the air flow can be regarded as aerodynamically smooth. As wind velocity increases, sea surface is agitated and gravity waves develop gradually. The drag coefficient becomes in this range considerably greater than that for aerodynamically smooth flow. However, the steepness of the sea surface is limited by wave breaking and the mean square slope is always bounded so that the direct viscous stress remains to be appreciable. The air flow over the sea would be better described as transitional between smooth and rough flows.

Introducing the steepness of the sea surface as a primary parameter for aerodynamic roughness, it follows from dimensional reasoning,

$$\frac{gz_0}{u_*^2}=\Psi\left[\frac{u_*^3}{g\nu},\ \frac{gH}{u_*^2},\ \left(\frac{H}{L}\right)^2\right].$$

In the extreme case of fully arisen sea with infinitely large fetch and duration of time, the power spectrum of surface waves will be determined only by u_* and g, the acceleration of gravity, so that parameters gH/u_*^2 and $(H/L)^2$ are regarded as constant. For sufficiently high

* Received September 20, 1969
** Institute of Coastal Oceanology, National Research Center for Disaster Prevention, Science and Technology Agency

wind in addition, one expects that the molecular viscous stress at the surface becomes small and that only in this limiting case the following Charnock's (1955) formula,

$$\frac{gz_0}{u_*^2}=\text{const},$$

is applicable asymptotically. Now, the steepness of the swells propagated from elsewhere is always small and they contribute no remarkable effect to the roughness of the sea. The major part is mainly due to the higher frequencies of the spectrum. Assuming the equilibrium range of the spectrum as suggested by PHILLIPS (1958), we could represent $(H/L)^2$ as a function of gH/u_*^2 and we propose here a formula describing the following relationship,

$$\frac{gz_0}{u_*^2}=\Phi\left(\frac{u_*^3}{g\nu},\ \frac{gH}{u_*^2}\right),$$

using the empirical relation between u_*z_0/ν and $(H/L)^2u_*H/\nu$ conjectured from rough flow over a rigid surface.

2. Equivalent roughness of a rigid suface having arbitrary roughness elments

From Nikuradse's experiments on flow through circular pipes with walls of uniform sand-grain roughness, it is concluded that for $u_*H_s/\nu<5$ the effect of $u_*\delta/\nu$ is not small, but that for $u_*H_s/\nu>55$ we have a fully rough wall condition, with no effective viscous sublayer.

For aerodynamically smooth surface, the so-called semilogarithmic law of mean velocity distribution is well established,

$$\frac{U}{u_*}=\frac{1}{\kappa}\ln\frac{u_*z}{\nu}+B, \qquad (1)$$

where z is taken vertically upwards and its origin is assumed to lie near the mean level of roughness elements comparing the volume transport of pipe flow having smooth and rough surfaces each other. Here, κ and B are constant and assumed as follows,

$$\kappa=0.4,\ B=5.5\,.$$

For tubulent flow over uniform sand-grain roughness, it is also known,

$$\frac{U}{u_*}=\frac{1}{\kappa}\ln\frac{z}{H_s}+B_s\,, \qquad (2)$$

where B_s is another constant and estimated in extreme case of completely rough flow as,

$$B_s=8.5\,.$$

It is noticed here that the value of B_s is in general not constant but a function of u_*H_s/ν as demonstrated by SCHLICHTING (1968). For smooth flow, we have from (1) and (2),

$$B_s=\frac{1}{\kappa}\ln\frac{u_*H_s}{\nu}+B\,. \qquad (3)$$

In the transitional régime between smooth and completely rough flow, we notice evidently from experiments by SCHLICHTING the region in which roughness function B_s changes more slowly with u_*H_s/ν than for smooth flow as expected from (3).

Now, the majority of experimental results are represented in the form for $z\gg z_0$,

$$\frac{U}{u_*}=\frac{1}{\kappa}\ln\frac{z}{z_0}\,. \qquad (4)$$

Comparing (4) with (1) we obtain for smooth flow,

$$\frac{u_*z_0}{\nu}=e^{-\kappa B}\approx 0.11\,. \qquad (5)$$

For completely rough flow, on the contrary, we get from (2) and (4),

$$\frac{u_*z_0}{\nu}=e^{-\kappa B_s}\frac{u_*H_s}{\nu}\approx 0.0334\frac{u_*H_s}{\nu}\,. \qquad (6)$$

The above considerations are only applicable to the uniform sand-grain roughness. For turbulent flow over arbitrary roughness elements with mean height H, we could expect also universal relationship from dimensional reasoning,

$$\frac{U}{u^*}=\frac{1}{\kappa}\ln\frac{z}{H}+B_1\,. \qquad (7)$$

It is noticed however that roughness function B_1, is somewhat different from B and B_s in (1) and (2). CLAUSER (1956) and HAMA (1954) proposed a formal representation for mean velocity distribution over arbitrary roughness elements as follows,

$$\frac{U}{u_*}=\frac{1}{\kappa}\ln\frac{u_*z}{\nu}+B-\frac{\Delta U}{u_*}, \qquad (8)$$

where $\Delta U/u_*$ shows the vertical shift in the mean velocity distribution and in two limiting cases it is given by,

$$\frac{\Delta U}{u_*}=\begin{cases}0 & ;\ \text{smooth}\\ \dfrac{1}{\kappa}\ln\dfrac{u_*H}{\nu}+B-B_1; & \text{rough}\,.\end{cases} \qquad (9)$$

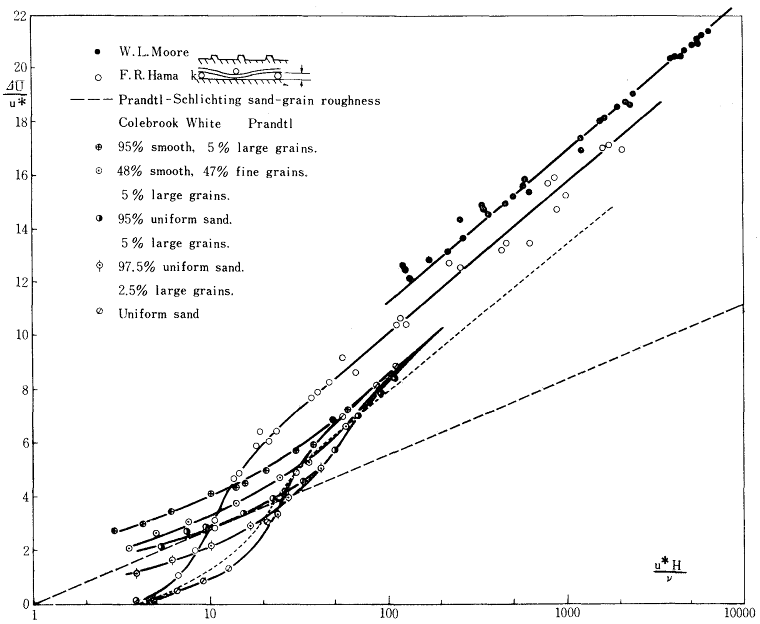

Fig. 1. Effect of wall roughness on the shift of the velocity distribution profile, reproduced from Clauser's (1956) publication. Lower dashed line is added to show the modification by (20a).

Introducing (9) in (8) we get again (1) and (7) for flow over smooth and rough surfaces respectively.

The values of $\Delta U/u_*$ for quite different type of roughness have been determined experimentally. Fig. 1 is reproduced from Clauser's (1956) publication. It is seen obviously that the above mentioned critical values $u_*H/\nu=5$ and 55 are valid only for uniform sand-grain roughness and that B_1 is by no means a universal function of u_*H/ν but dependent closely on the type of roughness, *i.e.*, B_1 is not a constant but some function of shape, size and distribution pattern of roughness elements.

Hitherto it has been unknown for us how to formulate parameter(s) to express the effect of such a roughness pattern. Only for completely rough flow we could derive equivalent roughness pattern comparing (7) with (2) as follows,

$$\frac{H_s}{H}=\exp\left[\kappa(B_s-B_1)\right]. \qquad (10)$$

It is noticed that H_s is independent of u_*H/ν only in the region of completely rough flow. Substituting (10) into (9) we have also,

$$\frac{\Delta U}{u_*}=\frac{1}{\kappa}\ln\frac{u_*H_s}{\nu}+B-B_s. \qquad (10a)$$

Now the question is to find a parameter characterizing arbitrary roughness pattern. In Fig. 2 is shown the relationship between H_s/H and $(H/L)^2$ calculated from Schlichting's (1968) experimental data. For all type of roughness pattern shown in Fig. 2 we get approximately,

$$\frac{H_s}{H}=\alpha\left(\frac{H}{L}\right)^2, \qquad (11)$$

where α takes the same value for roughness type No. 1-No. 3, but it is about one order larger for type No. 4,

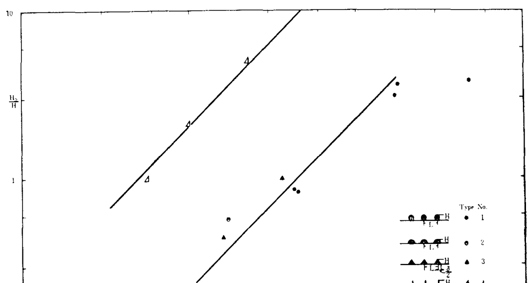

Fig. 2: Results of measurements by SCHLIGHTING (1968) on regular roughness patterns in regard to equivalent sand roughness.

$$\alpha \doteqdot \begin{cases} 23\,; & \text{roughness type No. 1–No. 3} \\ 210; & \text{No. 4.} \end{cases}$$

Now, the roughness pattern No. 3 may be expanded in Fourier series,

$$\frac{H}{\pi}\left[\frac{1}{4}kd + kd\sum_{n=1}^{\infty}\frac{1-\cos\left(n\frac{kd}{2}\right)}{\left(n\frac{kd}{2}\right)^2}\cos(nkx)\right],$$

where d denotes the width of triangular roughness elements as cited in Fig. 2. Then the slope of each wave number component is given by,

$$s_n = \frac{H_n}{L_n} = \frac{1}{2\pi}nkH_n = \frac{kH}{\pi^2}\frac{1-\cos\left(n\frac{kd}{2}\right)}{n\frac{kd}{2}}.$$

It follows from the above formula,

$$\sum_{n=1}^{\infty} s_n^2 = \left(\frac{kH}{\pi^2}\right)^2\frac{1}{a^2}\sum\left[\frac{2}{n^2} - 2\frac{\cos(an)}{n^2} - \frac{\sin^2(an)}{n^2}\right], \qquad (12)$$

where

$$a = \frac{kd}{2}.$$

The right hand side of (12) is not convergent, but for sufficiently large n we get

$$\sum_{n=1}^{\infty}\frac{1}{n^2} = \frac{\pi^2}{6},$$

then we get after some algebra,

$$\sum_{n=1}^{\infty} s_n^2 \sim \left(\frac{kH}{\pi^2}\right)^2\frac{\pi}{kd}.$$

If it is broadly assumed that the roughness pattern No. 4 corresponds to the roughness pattern No. 3 in which d is reduced one order smaller, then we could expect for mean square slope $\bar{s}^2$

$$[\bar{s}^2]_{\text{No. 4}} \sim 10[\bar{s}^2]_{\text{No. 3}}.$$

At any rate we could conjecture the following relation even if it is not yet confirmed experimentally,

$$\frac{H_s}{H} = \gamma\bar{s}^2. \qquad (14)$$

Comparing (14) with (10) we obtain,

$$\exp(-\kappa B_1) = \gamma\exp(-\kappa B_s)\bar{s}^2. \qquad (15)$$

From (4) and (7) it follows also,

$$\frac{z_0}{H} = \exp(-\kappa B_1). \qquad (16)$$

Comparing (15) with (16) we get finally,

$$\frac{u_* z_0}{\nu} = \gamma\exp(-\kappa B_s)\frac{u_* H}{\nu}\bar{s}^2$$
$$= \beta\frac{u_* H}{\nu}\left(\frac{H}{L}\right)^2;\ \beta = \alpha\exp(-\kappa B_s). \qquad (17)$$

For completely rough flow $B_s = 8.5$ and if we use the value of α from Schlichting's experiments for roughness type No. 1–No. 3, we get $\beta \doteqdot 0.77$

3. Roughness of the sea surface

Formula (17) is derived from artificial regular roughness pattern of a rigid surface and especially from the experiments carried by SCHLICHTING having rather large mean square slope.

For a rigid surface H/L is independent of $u_* H/\nu$ but for the sea surface, as later shown, it is a function of $u_* H/\nu$ and bounded by wave breaking. Then we expect that the variation of $u_* z_0/\nu$ is gentler than for a rigid surface.

Fig. 3 shows the experimental results of KUNISHI (1963) and HAMADA (1963) obtained in water-tunnel. The scatter of observed values is considerable but we could infer,

$$\frac{u_* z_0}{\nu} = b\sqrt{\frac{u_* H}{\nu}\left(\frac{H}{L}\right)^2};$$
$$\frac{u_* H}{\nu}\left(\frac{H}{L}\right)^2 \geqslant 10^{-4}, \qquad (18)$$

where b is constant and given experimentally,

$$b \doteqdot 10.$$

From the above empirical formula we could conclude that the wind disturbed sea surface is aerodynamically neither smooth nor rough but remains in transitional régime. Now we assume

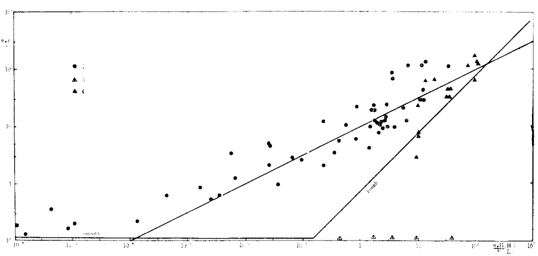

Fig. 3. Dependence of the roughness parameter on wind caused waves and on wave slope. 1) experimental data from KUNISHI (1663), 3) observed data from TAKAHASHI (1558), 4) experimental data from HAMADA (1963).

the same relation as (11) for the sea surface but with different constant of proportionality α', then it follows from (17) and (18),

$$\exp(\kappa B_s)=\frac{\alpha'}{b}\sqrt{\frac{u_*H}{\nu}\left(\frac{H}{L}\right)^2}. \quad (19)$$

Substituting (11) into (19) we get equivalent roughness function B_s of the sea surface as follows,

$$B_s=\frac{1}{2\kappa}\ln\frac{u_*H_s}{\nu}+D;\ D=\frac{1}{2\kappa}\ln\frac{\alpha'}{b^2}. \quad (20)$$

Comparing (20) with (3) it is seen that the equivalent sand roughness function B_s of a disturbed sea surface increases with u_*H_s/ν more gradually than for a rigid smooth surface. If we substitute (20) into (10a) we have also,

$$\frac{\Delta U}{u_*}=\frac{1}{2\kappa}\ln\frac{u_*H_s}{\nu}+B-D$$
$$=\frac{1}{2\kappa}\ln\frac{u_*H}{\nu}+B-D$$
$$+\frac{1}{2\kappa}\ln\left[\alpha'\left(\frac{H}{L}\right)^2\right]. \quad (20a)$$

Thus $\Delta U/u_*$ changes more slowly compared with completely rough flow. It is similar to Colebrook's data in Fig. 1 for intermediate wall condition not hydraulically rough but direct viscosity effect is still sappreciable. It may be also resembled to the transitional region of Prandtl-Schlichting sand-grain roughness for $5<u_*H/\nu<10$.

Thus the assumption of the form (11) with different constant of proportionality for a disturbed sea surface and empirical formula (18) would be better to describe a sea surface condition.

Mean square slope of wind caused sea surface is represented by definition,

$$\bar{s}^2=\int \boldsymbol{\kappa}^2S(\boldsymbol{\kappa})d\boldsymbol{\kappa}=\frac{1}{g^2}\int_0^\pi d\theta\int_0^\infty \sigma^4S(\sigma)d\sigma, \quad (21)$$

where $S(\boldsymbol{\kappa})$ denotes wave number spectrum of the sea surface. Contribution to $\bar{s}^2$ is mainly due to higher wave number range, we assume now,

$$S(k)=\begin{cases}\frac{A}{\pi}k^{-4};\ k_0\leqslant k\leqslant k_N\\ 0\ ;\ k<k_0,\ k>k_N\ ,\end{cases}$$

where k_0 is optimum wave number of the power spectrum and k_N is cut-off wave number. Introducing in (21) and integrating both in direction and wave number, we get easily,

$$\bar{s}^2=A\ln\frac{k_N}{k_0}. \quad (22)$$

Total power of wind waves is represented approximately for this case,

$$E=2\int_{k_0}^{k_N}S(\boldsymbol{\kappa})d\boldsymbol{\kappa}\doteqdot\frac{A}{k_0^2}. \quad (23)$$

Introducing the dispersion relationship in the gravity waves, $\sigma^2=gk$, we get finally from (22) and (23),

$$\bar{s}^2=\frac{A}{2}\ln\left(k_N^2\frac{E}{A}\right) \quad (24)$$

$$H\approx\sqrt{\pi(1-\varepsilon^2)E}, \quad (25)$$

where ε shows the parameter indicating the spectrum width. Introducing (25) into (24) it follows immediately,

$$\bar{s}^2\approx\frac{2}{3}A\ln\left[\alpha_1^3\left(\frac{gH^3}{\nu^2}\right)^{1/2}\right]$$
$$=\frac{2}{3}A\ln\left[\alpha_1^3\frac{u_*^3}{g\nu}\left(\frac{gH}{u_*^2}\right)^{3/2}\right], \quad (26)$$

where $\alpha_1=[\pi A(1-\varepsilon^2)]^{-1/4}\left(\frac{\nu^2k_N^3}{g}\right)^{1/6}$.

Now, we denote the n-th moment of the spectrum by,

$$M_n=\int_0^\infty \sigma^nS(\sigma)d\sigma,$$

we get then from the statistical theory of RICE (1944)

$$\left(\frac{T_0}{2\pi}\right)^2=\frac{M_0}{M_2},\ \left(\frac{T_p}{2\pi}\right)^2=\frac{M_2}{M_4}.$$

Introducing into (21) we have a representation for the mean square slope,

$$\bar{s}^2=(2\pi)^4\frac{1-\varepsilon^2}{2}\frac{E}{g^2T_p^4}, \quad (27)$$

where ε is defined by,

$$\varepsilon^2=1-\left(\frac{T_p}{T_0}\right)^2.$$

When we denote L, mean wave length, defined as follows,

$$L=\frac{gT_p^2}{2\pi}, \quad (28)$$

we get from (25) and (27) the slope of the mean wave,

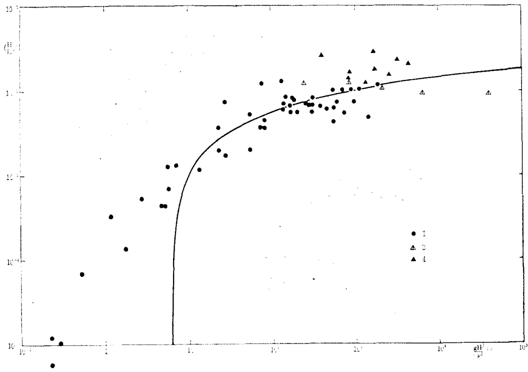

Fig. 4. Dependence of wave slope on wave height. Symbols as for Fig. 3.

$$\left(\frac{H}{L}\right)^2=\frac{1}{2\pi}\bar{s}^2\,. \qquad (29)$$

In reality observed mean wave length L may be somewhat smaller than the value estimated from (28). At any rate we obtain from (26) and (29),

$$\left(\frac{H}{L}\right)^2\approx\frac{A}{3\pi}\ln\left[\alpha_1{}^3\left(\frac{gH^3}{\nu^2}\right)^{1/2}\right]. \qquad (30)$$

Fig. 4 shows the observed results. The curve is drawn by (30) on the assumption that

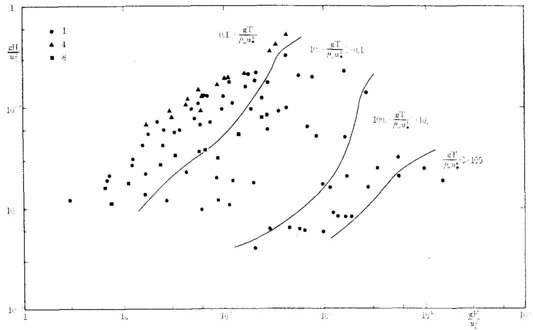

Fig. 5. Fetch-Graph referred to friction velocity. 8) experimental data from HIDY-PLATE. Other symbols as for Fig. 3.

$$\alpha_1=0.55;\ A=1.8\times10^{-2}.$$

The value of A is about three times larger than previously estimated values (PHILLIPS, 1966). It may be partly due to the overestimated value of L using (28). However, the curve fits well observed values for $gH^3/\nu^2\geqslant10$. It corresponds to the mean wave height 0.01 cm for $\nu=0.15$ and $g=980$. The discrepancy for $gH^3/\nu^2<100$ is due to the effect of capillary waves. This effect is remarkably observable in the so-called

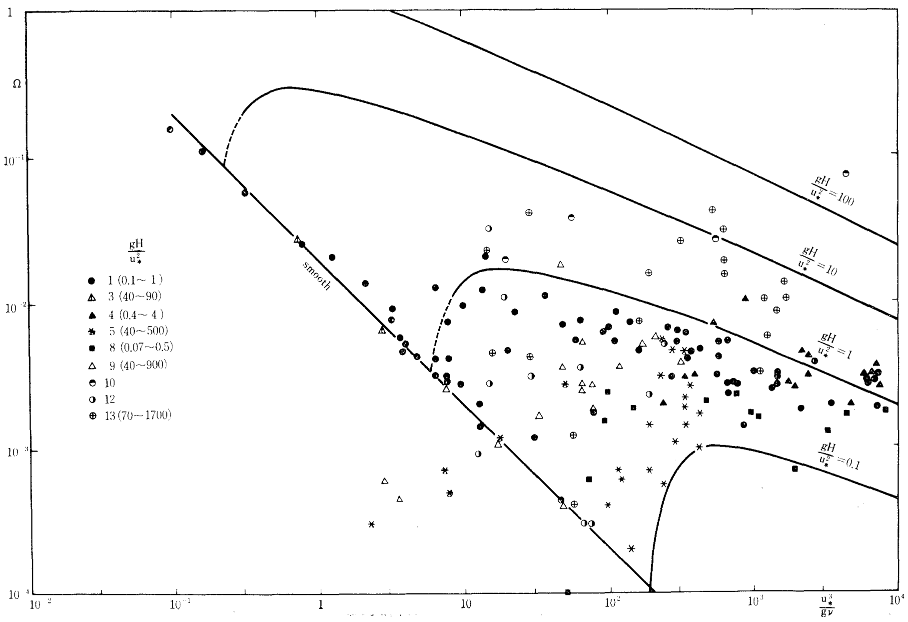

Fig. 6. Dependence of shear parameter on friction velocity and on wind-caused wave height. 5) observed data from HASSE (1968), 9) observed data from NAN-NITI *et al.* (1968), 10) observed data from VINOGRADOVA (1959), 12) observed data from KUZNECHOV (1965), 13) observed data from SNOPKOV and ROMANOV (1965). Other symbols as for Fig. 5.

Fetch-Graph in Fig. 5. As a characteristic parameter for the capillary waves, we may take $gT/\rho_w u_*^4$. When the value of this parameter becomes larger than 10 for small u_*, the mean wave height is obviously influenced by surface tension and reduced even for large fetch.

As is shown by LONGUET-HIGGINS (1969) H/L is also bounded and smaller than $1/2\pi$. Inserting this value in the left hand side of (30) we get sufficiently large value for H as upper bound.

Now introducing (30) into (18) we obtain,

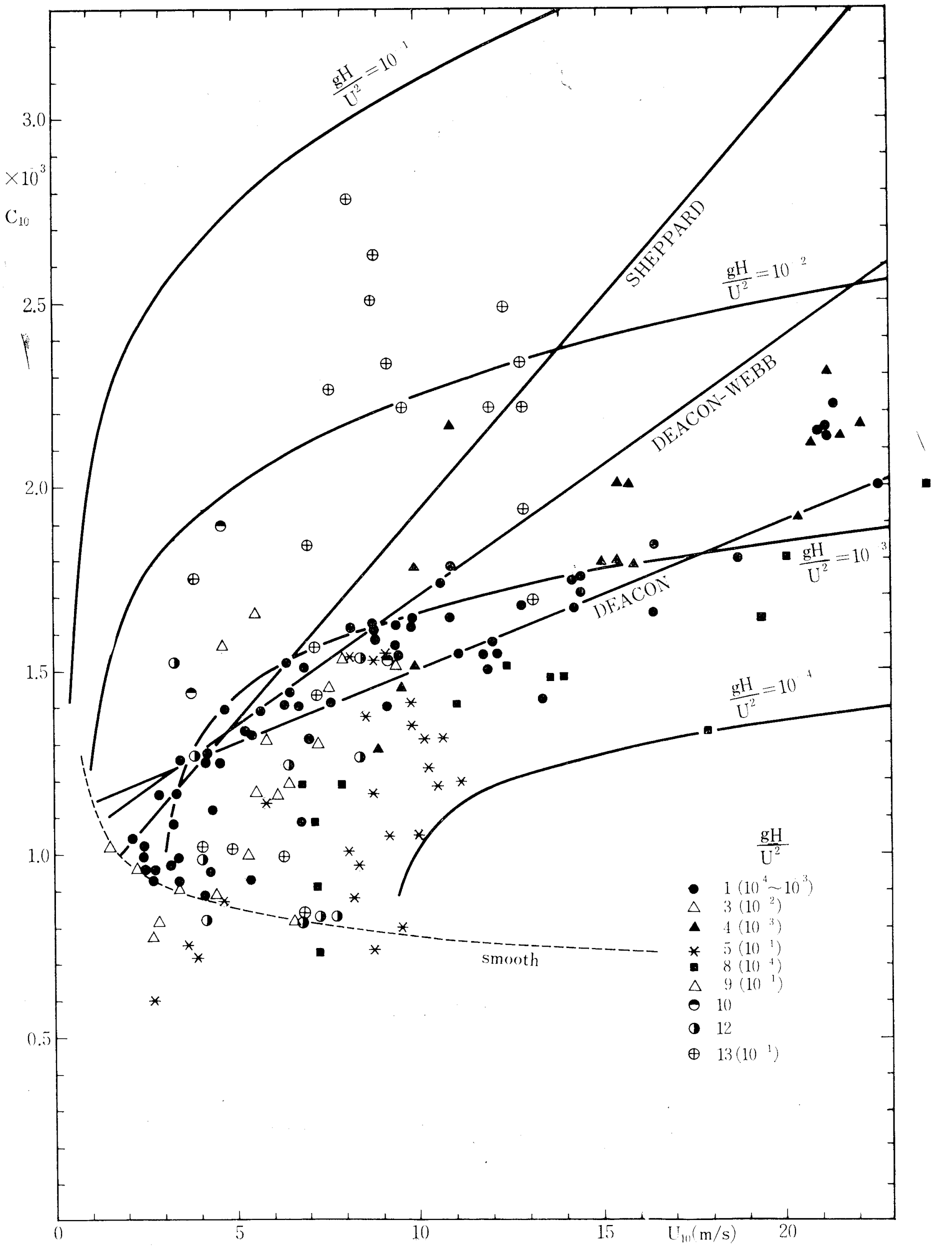

Fig. 7: Relation between drag coefficient and mean wind velocity over the sea surface with regard to wave height as parameter. Symbols as for Fig. 6.

$$\Omega=\kappa^2\frac{gz_0}{u_*^2}$$

$$=\kappa^2 b\sqrt{\frac{A}{3\pi}}\sqrt{\frac{\frac{gH}{u_*^2}}{\frac{u_*^3}{g\nu}}}$$

$$\sqrt{\ln\left\{\alpha_1^3\frac{u_*^3}{g\nu}\left(\frac{gH}{u_*^2}\right)^{3/2}\right\}} \qquad (31)$$

Fig. 6 is the representation of the observed results of Ω as function of $u_*^3/g\nu$ for various values of gH/u_*^2. The curve is drawn by (31) assuming

$$b=10,\ \kappa=0.4,\ A=0.018,\ \alpha_1=0.55\,.$$

For aerodynamically smooth flow it follows from (5),

$$\Omega=\kappa^2 e^{-\kappa B}\frac{g\nu}{u_*^3}\,.$$

Obviously Ω depends not only on $u_*^3/g\nu$ but also on gH/u_*^2. Calculated values of Ω from (31) fit well experimental data in wind-water tunnel. However for field observations, the observed values are rather scattered and show somewhat larger values of gH/u_*^2 than expected from (31). It is partly due to the overestimation of H in the field observations. Average height H must be taken as mean wave height caused only by local wind, excluding the swell propagated from elsewhere. At any rate we see in Fig. 6 that for a definite value of $u_*^3/g\nu$, Ω increases with gH/u_*^2 which is originally dependent function of fetch (gF/u_*^2) and duration (gt/u_*). In the stage of wave development Ω then increases with gt/u_*. When we assume Miles' (1957) régime for wave generation, we could conjecture that the energy transfer coefficient of MILES becomes several times larger for earlier stage due to rather small value of Ω.

Drag coefficient is defined as follows,

$$C_{10}=\left(\frac{u_*}{U_{10}}\right)^2.$$

Introducing the above formula into (4) we get,

$$\Omega=\frac{\kappa^2}{C_{10}}\exp\left(-\frac{\kappa}{\sqrt{C_{10}}}\right)\left(\frac{gz^3}{\nu^2}\right)^{1/3}\left(\frac{U^3}{g\nu}\right)^{-2/3}. \qquad (32)$$

From (31) it follows similarly,

$$\Omega=b\sqrt{\frac{A}{3\pi}}\frac{\kappa^2}{C_{10}^{5/4}}\left(\frac{\frac{gH}{U^2}}{\frac{U^3}{g\nu}}\right)^{1/2}$$

$$\sqrt{\ln\left\{\alpha_1^3\left(\frac{U^3}{g\nu}\right)\left(\frac{gH}{U^2}\right)^{1/2}\right.}, \qquad (33)$$

equating both representations, we get finally,

$$C_{10}^{1/4}\exp\left(-\frac{\kappa}{\sqrt{C_{10}}}\right)$$

$$=b\sqrt{\frac{A}{3\pi}}\left(\frac{\nu^2}{gz^3}\right)^{1/3}\left(\frac{gH}{U^2}\right)^{1/2}\left(\frac{U^3}{g\nu}\right)^{1/6}$$

$$\sqrt{\ln\left\{\alpha_1^3\frac{U^3}{g\nu}\left(\frac{gH}{U^2}\right)^{1/2}\right\}}. \qquad (34)$$

Fig. 7 shows the observed results of drag coefficients. The straight lines are empirically determined by SHEPPARD (1958), DEACON-WEBB (1962) and DEACON (1962)

$$C_{10}=(0.8+0.11U_{10})\times10^{-3} \quad : \text{SHEPPARD}$$
$$=(1.0+0.07U_{10})\times10^{-3} \quad : \text{DEACON-WEBB}$$
$$=(1.10+0.04U_{10})\times10^{-3} \quad : \text{DEACON}$$

The curves are drawn using (34) for various values of gH/U_{10}^2. It is noticed that C_{10} is remarkably dependent on wave height caused by local wind and that for a definite value of gH/U_{10}^2, it changes quite slowly with U_{10}.

References

CARTWRIGHT, D. E. and M. S. LONGUET-HIGGINS (1956): The statistical distribution of the maxima of a random function, Proc. Roy. Soc. London, A, **237**, 212-232.

CHARNOCK, H. (1955): Wind stress on a water surface. Quart. J. R. Met. Soc., **81**, 639-640.

CLAUSER, F. H. (1956): "Advances in Appl. Mech." **4**, 1-51.

DEACON, E. L. (1962): The drag of the wind on the sea. Mitteil. Inst. Meereskunde Hamburg **1**, 385-397.

DEACON, E. L. and E. K. WEBB (1962): Interchange of properties between sea and air, small scale interaction. in "The Sea", Hill(ed.), 43-87.

HAMA, F. R. (1954): Boundary layer characteristics for smooth and rough surfaces. Trans. Soc. Naval Architects Marine Engrs., **62**, 333-358.

HAMADA, T. (1963): An experimental study of development of wind waves. Rep. Port and Harbour Tech. Res. Inst., No. 2, 1-41.

HASSE, L. (1968): Zur Bestimmung der vertikalen Transporte von Impuls und fuehlbarer Waerme in der wassernahen Luftschicht ueber See. Hamburger Geophysikalische Einzelschriften, Nr. 11, pp. 70.

HIDY, G. M. and E. J. PLATE (1966): Wind action on water in a laboratory channel. Jour. Fluid Mech., **26**(4), 651-687.

KUNISHI, H. (1963): An experimental study on the generation and growth of wind waves. Disaster Prevention Res. Inst., No. 61, 1-41.

KUZNECHOV, O. A. (1965): On the wind profile formation in the air layer overlying the sea surface. Trans. (Trudy) Inst. Oceanol. Acad, Sci, USSR, **78**, 158-191.

LONGUET-HIGGINS, M. S. (1969): On wave breaking and equilibrium spectrum of wind-generated waves, Proc. Roy. A, **310**, 151-159.

MILES, J. W. (1957): On the generation of surface waves by shear flows, Jour. Fluid Mech., **3**(2), 185-204.

NAN-NITI, T., A. FUJIKI and H. AKAMATSU (1968): Micro-meteorological observations over the sea (1), Jour. Oceanogr. Soc. Japan, **24**(6), 281-294.

PHILLIPS, O. M. (1958): The equilibrium range in the spectrum of wind-generated waves. Jour. Fluid Mech., **4**, 426-434.

PHILLIPS, O. M. (1966): "The dynamics of the upper ocean". Cambridge Univ. Press, pp. 261.

RICE, S. O. (1944): Mathematical analysis of random noise. in "Noise and Stochastic Processes", Dover Publications Inc., 133-294.

SCHLICHTING, H. (1968): "Boundary-layer theory" (six edition), McGraw-Hill, pp. 747.

SHEPPARD, P. A. (1958): Transfer across the earth's surface and through the air above. Quart. J. R. Met. Soc., **84**, 205-224.

SNOPKOV, V. G. and A. ROMANOV (1965): On the turbulent exchange in the surface layer over the ocean. Trans. (Trudy) Inst. Oceanol. Acad. Sci. USSR, 78, 203-226.

TAKAHASHI, T. (1958): Micro-meteorological observations and studies over the sea. Mem. of the Faculty of Fisheries, Kagoshima Univ., 6, 1-46.

VINOGRADOVA, O. P. (1969): Tangential wind stress above a disturbed sea surface. Izv. Geophys. Ser., 1646-1655.

海面の空気力学的粗度

岩田憲幸

要旨: 人工的に作られた粗面上の SCHLICHTING の実験結果を使用すると，NIKURADSE の砂粒の場合に等価な粗度と，考察している粗面の凹凸の高さの比は，粗面自体の自乗平均傾度に比例するとみなすことができる。これは粗な固定壁上で得られた結果であるが，波立っている水面上の実験結果を整理すると水面の粗度を示すパラメーター u_*z_0/ν は，やはり波面の傾斜の関数となる。ただしその関係は，完全に粗である固定壁の場合から期待されるものと異なって，空気力学的に滑らかである場合と粗である場合の中間にある。

この関係を経験式で近似して，砂粒の場合と等価な粗度を求めると，固定壁の場合に換算してもやはり滑かな場合と粗な場合の中間の値をとる。以上のことから波立っている水面は，空気力学的に滑かではないが，粘性が無視できるほど粗でもないことがわかる。

水面の場合は，固定壁の場合と異なって自乗平均傾度は，波高と無関係ではない。波浪のスペクトルの平衡領域に −5 乗則を適用して上述の経験式を利用すると，風の shear parameter gz_0/u_*^2 が，波高と u_* によってどのように変化するかを求めることができる。この量は u_* を一定とすると，波高と共に増大する。したがって，風浪発生初期においては，従来考えられていたものより小さい値をとるから，風から波へのエネルギー伝達係数は逆に大さくとらなければならないことになる。

同様な推論から，抵抗係数が風速のみならず，波高の関数であることが導かれる。室内実験から求められた経験式を使用した結果であるから，抵抗係数に関する室内実験の結果とよく一致するのは当然であるが，この結果を実際の海面に適用してもそれ程無理ではないと考えられる。

La mer (Bulletin de la Société franco-japonaise d'océanographie)
Tome 7, N° 4, Novembre 1969

The Larval Development of *Macrobrachium nipponense* (De Haan) reared in the Laboratory*

KWON Chin Soo** and Yutaka UNO**

Résumé: Les auteurs élèvent la larve de *Macrobrachium nipponense* (De Haan) dans un bassin expérimental à 27,8°～28,2°C de température et à 4,56～5,15‰ de chrolinité. La larve d'*Artemia saline* est donnée comme appât. Elle se métamorphose à la postlarve par neuf périodes de zoé. Sa forme à chaque période est illustrée et comparée avec celle de *Macrobrachium rosenbergi* (De Man). Elles sont distinguées par les mandibules, les premières maxilles et la couleur du troisième somite abdominal.

1. Introduction

The prawn, *Macrobrachium nipponense* (De Haan) is very commonly met with in brackish and fresh waters of Far East region, especially China, Formosa, Japan and Korea (HOLTHUIS, 1950). The species is one of the important commercial fresh water prawns in Japan and Korea.

Recently, interest has been shown in the possibilities of the culture for mass-production of the genus in the world. *Macrobrachium carcinus* has been reported by LEWIS *et al.* (1965) and *M. rosenbergi* by LING (1961, 1962) and UNO and KWON (1969).

The taxonomical and ecological studies of the prawn has been reported by KUBO (1940, 1949, 1950). However, there is little evidence on larval development so far except of Icho's information (1940). The present paper is dealt with larval development of the species reared in the laboratory, as the first place of the propagation on this prawn.

Our acknowledgements are due to Mr. H. YAMAKAWA, assistant of the University, for providing assistance in setting apparatus of this work.

2. Materials and method

Ovigorous female prawns used for this work were obtained from the Lake, Kasumiga-ura, Ibaragi Prefecture and removed our university for culture; after rearing and being adapted in the aquaria under the controlled conditions, we were able to breed larvae of new generation. Culture methods have already described (KWON and UNO, 1968). Throughout the aquaria were kept continuously in constant temperature 27.8～28.2°C, salinity 4.56～5.15 ‰ Cl.

Individuals of zoea larvae of the various stages were placed one in 300 m*l* jar to assure of molting periods. After assurance of molting the species were anesthetized with 1% T-cain solution, and then placed on slideglass for observation. After dissection all parts of the larval appendages, they were sketched by camera lucida. The length of each appendage was measured with a micrometer.

3. Results

The eggs are slightly oval in shape, measuring from 0.54×0.67 mm change to 0.56×0.92 mm on average and their color bright-gray and change from right to dark color owing to advance of developmental embryo. The larvae emerge from the eggs as zoea.

First zoea: body length, 2.06 mm, from the posterior margin of telson to the base of suborbital spine and carapace length 0.53 mm on average. The cephalothorax is covered with the unarmed carapace, while rostrum projects almost horizontally. Six abdominal somites, the last is not separated from telson, which is thin, much laterally dilated and spatular in structure. Eyes are sessile.

Posterior margin of spatular expansion armed

* Received October 5, 1969
** Ecological Laboratory, Tokyo University of Fisheries

with seven pair of spines, and still no segment between sixth somite and telson, almost with chromatophore at rudimentary anus. Outer two pair of telson spines devoid of branching cilia on outer margin, while the remaining pair with cilia on both margins (Pl. VII, 8).

The prominent chromatophores locate on the dorso-lateral part of third abdominal somite, base of eyes, anal part and instinct light pink pigment on mid-ventral carapace; abdominal chromatophores consisted of one expansive at mid-portion and two contractive at outer portion, outer two develop more distinctly in future stages. This stage larvae are almost transparent white.

Antenna (Pl. II, 1) biramous; basis segmented, with a minute spine on the inferior surface; flagellum unisegmented, shorter than scale, with a long terminal plumose seta and a small spine at the distal end; scale foliaceous in shape, a little concaved near the top on outer margin, armed with one plumose and a single setae on outer margin, and eight setae on the anterior and inner margin, and one rudimental minute seta at mid-portion; scale of a long basal segment, which is convex on inner side, and four short terminal segments.

Antennule (Pl. II, 11) simple; peduncle unsegmented; basal segment bears a long stout plumose seta terminally, a little outer flagellum with four aesthetes and a slender plumose seta.

Mandible (Pl. III, 1) without palp, so simple; incisor process with incomplete two teeth at tip; molar process without toothed cutting edge; a movable tooth in angle between molar and incisor processes. First maxilla (Pl. III, 11) uniramous, consisting of three lobes; basis with two teeth and a spine; coxa with five spines covered with cuticular membrane; exopod tiny, palp-like, with two rudimental minute spines terminally, without seta. Second maxilla (Pl. III, 21) biramous, plate-like; protopod three-lobed, armed with three, three and three setae; endopod unsegmented, bears two setae on a lobe near the proximal end and a seta terminally; exopod a flattened gill bailer with three anteriorly, one laterally and one plumose setae posteriorly.

First maxilliped (Pl. IV, 1) biramous; protopod rudimentary folded, armed with three or four medially directed seta on inner margin; endopod also unsegmented, armed with four plumose setae on terminal extremity; exopod with apicial setae, longer than endopod. Second maxilliped (Pl. IV, 11) biramous; coxa reduced; protopod with a seta on inner margin; endopod three-segmented, with a strong at the junction of ultimate and penultimate segments, two small setae at near distal portion and strong terminal claw; the proximal segment is longer than the others; exopod with four apical setae, longer than endopod. Third maxilliped (Pl. IV, 21) biramous; longer than second maxilliped, almost similar to the former in structure but the following only difference: basal segment armed with two setae on inner margin; merus with two strong setae at the junction of ultimate and penultimate segments.

First and second pereiopod (Pl. V, 1) rudimentary, biramous; the former somewhat longer than the latter in size.

Second zoea: body length 2. 27 mm, carapace length 0. 53 mm. Differs from the previous larva in the followings: chromatophores of third dorso-abdominal somite and the anal portion more extensive. Carapace with a pair of branchiostegal and sub-orbital spines. Telson (Pl. VII, 9) armed with eight pair of setae, of which the last outer pair is devoid of outer branching cilia. Rudimentary articulation of uropod appears at the last period of this stage; fifth somite of abdominal pleura is pointed posteriorly. Eyes stalked, with chromatophores at base of stalk.

Antennal scale (Pl. II, 2) longer than flagellum, with a seta on outer margin; flagellum with 1 long, 2 small setae and a spine at terminal end. Antennule (Pl. II, 12) with two-segmented peduncle, bearing a long stout and 3 short plumose setae on distal end of proximal segment, and 4 short plumose setae at the articulation between segments; peduncle flagellum with 4 aesthetes and 1 slender seta at the distal end.

Mandible (Pl. III, 2) without palp; incisor process with 3 teeth at tip; molar process with 5 fine-toothed cutting edge, 2 movable teeth in angle between molar and incisor processes. First maxilla (Pl. III, 12) uniramous, consisting of 3 lobes; coxa with 5 inwardly directed spines; basis with 3 spines and 4 teeth; exopod simple, palp-liked with a rudimentary minute terminal seta. Second maxilla (Pl. III, 22) biramous, plate-like; protopod three-lobed, armed with 4, 3 and 3 plumose setae; endopod unsegmented, more or less folded near the mid-portion, bears 2 setae on a lobe at mid-portion and a seta terminally; exopod a flattened gill bailer with 3 anteriorly, 2 plumose setae posteriorly.

First maxilliped (Pl. IV, 2) biramous; protopod unsegmented, folded only; primitive basis armed with 5 medially directed setae on inner margin, a seta near the folded portion; endopod unsegmented with 4 setae on terminal extremity; exopod with 4 apical setae, longer than endopod; epipod appear, not segmented. Second maxilliped (Pl. IV, 12) biramous; coxa reduced; protopod with a seta on inner margin; endopod three-segmented, with a strong and a small setae at the junction of ultimate and penultimate segments, ultimate segment with a seta at middle portion and 2 small slender setae near the distal end; exopod with 4 apical and 2 sub-apical setae. Third maxilliped (Pl. IV, 22) more advanced than previous stage in size, almost similar to the former stage in structure except for 2 strong setae at the junction of ultimate and penultimate segments; exopod with 4 apical and 2 sub-apical setae.

First pereiopod (Pl. V, 2) biramous; coxa reduced; somewhat longer than third maxilliped; endopod four-segmented, merus, carpus, propodus and dactylus, and more advanced strong claw than third maxilliped at the terminal end; merus bearing with 2 setae inner margin, a seta at the junction of carpus and propodus outer margin, 2 stout setae at the junction of propodus and dactylus, and a small slender seta near the terminal portion; basis armed with 2 setae on inner margin; exopod with 4 apical and 2 sub-apical setae. Second pereiopod (Pl. V, 12) biramous; coxa reduced; somewhat longer than first pereiopod, almost similar to first pereiopod; exopod shorter than endopod. Third and fifth pereiopod (Pl. VI, 2; Pl. VI, 17) both rudimentary; the former biramous, the latter uniramous; fourth pereiopod no appeared.

Third zoea: body length 2.61 mm, carapace length 0.58 mm. Differs from the former in the followings: carapace (Pl. I, 3) with a dorsal rostrum tooth and a pair of branchiostegal spines. Sixth abdominal somite separates from telson; all spines of telson (Pl. VII, 10) with branching cilia. Uropod biramous; endopod bare, rudimentary; exopod with 6 setae. Antennal scale (Pl. II, 3) two-segmented, armed with 13 plumose and a simple setae; flagellum with 2 segments and a short peduncle near the basis and 4 short setae at the terminal end. Antennular peduncle (Pl. II, 13) with 2 large plumose setae and 2 flagella at the terminal segment; inner flagellum small, with a setae; the outer with 4 aesthetes and a slender seta, and terminally near the prominance 4 short setae on the opposite side; proximal segment armed with a long stout plumose, 2 long at the mid-portion and about 4 small setae at the articulation of segment on the inner side, 2 setae sub-terminally on the outer side, about plumose short setae middle-laterally and one or two small setae on the prominance near the base, future stylocerite, on the inner side. Endopod of second maxilla (Pl. III. 23) with 5 anteriorly, 1 laterally and 2 setae posteriorly, one of two posterior setae longer and stouter than the other. Basis of first maxilliped (Pl. IV, 3) with 5 medially directed setae; endopod with a minute seta near the middle portion on inner side; exopod with 4 apical and 2 sub-apical plumose setae; epipod biramous uncompletely. Second maxilliped (Pl. IV, 13) more advanced; endopod four-segmented, with a strong and two setae; exopod with 4 apical and 2 sub-apical setae. Third maxilliped (Pl. IV, 23) biramous; coxa reduced; basis with 2 setae; endopod four-segmented, ischium and merus with 2 setae each, two stout spines at the junction of propodus and dactylus with a spine; of the 4 segments, the merus longer than the others; exopod with 4 apical and 2 sub-apical setae, longer than endopod. First and second pereiopod (Pl. V, 3; Pl. V, 13) biramous as in third maxilliped in shape except of difference from being armed with 3 spines at the junction of propodus and dactylus.

Fourth zoea: body length 3.07 mm, carapace length 0.70 mm. Differs from the former stage in the followings: light-pinkish chromatophores appear at the ventral portion of fourth abdominal somite; red chromatophores on merus, carpus and propodus of third maxilliped, first, second, fourth and fifth pereiopods endopods.

Carapace (Pl. I, 4) with 2 rostrum teeth. Telson (Pl. VII, 11) oblong and almost recutangular, with five pair posteriorly and a pair of spines laterally. Uropod (Pl. VII, 11) biramous; outer ramus with about 11 plumose setae and a small spine; inner ramus with about 8 setae. Antennal scale (Pl. II, 4) unsegmented at distal portion; disto-lateral tip pointed spine, somewhat concaved at distal end; blade with about 16 plumose setae. Antennule (Pl. II, 14) almost similar to the former stage in shape; terminal peduncle with 4 large plumose setae; two flagella distinctly; proximal peduncle with more setae at the articulation of segment than the former stage and 4 setae sub-terminally on the outer side; proximal segment with 10 plumose, 1 setae at the mid-lateral portion on inner side and about 6 setae on the prominance near the base.

Mandible (Pl. III, 4) incisor process with 3 teeth at tip; molar process with 3 fine-toothed cutting edge, 3 movable teeth in angle between molar and incisor processes. Second maxilla (Pl. III, 24) exopcd a flattened gill bailer with 7 anteriorly, 1 laterally and 3 setae posteriorly; two of them small and another large plumose setae. Second maxilliped (Pl. IV, 14) with 3 strong setae at the junction of ultimate and penultimate segments, two of them on inner margin and one on outer margin. Third maxilliped (Pl. IV, 24) almost similar to the former stage excepting of 3 strong setae at the junction of dactylus and propodus of endopod.

First and second pereiopod (Pl. V, 4; Pl. V, 14) more advanced. Third pereiopod (Pl. VI, 3) similars to the third maxilliped, being 2 strong setae at the junction of propodus and dactylus; exopod smaller than endopod; exopod armed with 4 apical and 2 sub-apical setae. Fifth pereiopod (Pl. VI, 19) uniramous; coxa reduced; merus with 2 setae and 1 short seta at the junction of ischium, propodus with 2 and 1 short setae at the junction of propodus and carpus and dactylus with 1 seta, terminated in a strong claw. Fourth pereiopod (Pl. VI, 10) biramous, rudimentary.

Fifth zoea: body length 3.71 mm, carapace length 0.88 mm. Differs from the former in the followings: chromatophores of fourth abdominal somite and locomotive appendages are advanced. Carapace with a seta on the first rostrum tooth (Pl. I, 5). Telson (Pl. VII, 12) more elongated, with five pair posteriorly and two pair of spines laterally, and terminal edge somewhat narrower than the basis. Rudimentary buds of pleopods appear (Pl. I, 5). Antennal flagellum two-segmented (Pl. II, 5), almost same as scale in length; scale with about 20 plumose setae. Peduncle segment of antennule (Pl. II, 15) with more setae around than the previous stage, 6 large sub-terminally on the outer side and about 9 setae on the prominance, stylocerite, and it's angle acute; proximal segment bears a tooth at the about mid-way on the ventral side. Molar process of mandible (Pl. III, 5) with 4 fine-toothed cutting edge. Coxa of first maxilla (Pl. III, 15) with 6 inwardly directed spines. Exopod of second maxilla (Pl. III, 25) with 8 anteriorly, 4 laterally and 4 setae posteriorly. First maxilliped (Pl. IV, 5) with 5 setae medially directed and 2 setae near the middle portion on inner margin of basis; exopod with 1 seta on outer side; epipod biramous. First and Second pereiopod (Pl. V, 5; Pl. V, 15) more developed, armed 2 spines in each at the articulation of propodus and carpus. Third pereiopod (Pl. VI, 4) more advanced, with 2 spines of carpus and 2 setae on inner margin of protopod. Fourth pereiopod (Pl. VI, 11) biramous, still uncomplete; endopod sometimes without apical and sub-apical setae, shorter than exopod. Fifth pereiopod (Pl. VI, 20) more advanced; dactylus with a stout spine on inner side, a seta at the articulation of dactylus and propodus; propodus with setae on inner side and 2 setae at the articulation of propodus and carpus. Uropod (Pl. VII, 12) more advanced, with more setae of both ramus,

Sixth zoea: body length 4.24 mm, carapace length 0.98 mm. Differs from the former stage in the followings: all appendages are advanced in size. Carapace bears 2 small setae under the first rostrum tooth (Pl. I, 6). Five pair of pleopods (Pl. VII, 1) appear, bare, biramous. Antennal flagellum (Pl. II, 6) two or three-segmented; almost similar in length as the scale; (Pl. II, 6) with about 22 setae; basis of antennal flagellum three-segmented; proximal segment armed with a seta on inner side. Antennular peduncle (Pl. II, 16) bears more setae at the articulation of proximal and sub-proximal segment increasing prominance setae at the mid-portion on the inner side, about 11 setae. Mandible (Pl. III, 6) with 5 movable teeth in angle between molar and incisor processes. First maxilla (Pl. III, 16) basis with 5 teeth and 3 spines, coxa with 6 inwardly directed spines. Second maxilla (Pl. III, 26) exopod a flattened gill bailer with about 22 setae, especially 4 posteriorly stout. First maxilliped (Pl. IV, 6) basis with 7 setae medially directed, 2 median setae near the middle portion on inner margin; exopod with about 3 setae near the proximal portion on outer side. Third maxilliped (Pl. IV, 26) with 2 setae at the articulation of propodus and carpus, merus with 2 setae. Endopod of first and second pereiopod (Pl. V, 6; Pl. V, 16) protubarant at inner distal corner, forming rudimentary chelae with dactylus and propodus; propodus with 2 at the articulation of propodus and carpus, 2 small at the distal of the protuberance and 3 setae near the articulation of carpus and propodus; merus with 3 setae; endopod with 4 apical and 2 sub-apical setae in each. Third pereiopod (Pl. VI, 5) biramous; endopod with 4 at the articulation of dactylus and propodus, 2 at the articulation of carpus and propodus, 2 on inner side of merus and 2 setae on basis; exopod developed in length, with 4 apical and 2 sub-apical setae, larger than fourth pereiopod. Fourth pereiopod (Pl. VI, 12) with 3 setae at the articulation of dactylus and propodus; endopod with 4 apical and 2 sub-apical setae, longer than exopod. Fifth pereiopod (Pl. VI, 21) more developed in size, with 2 setae at the articulation of carpus and merus. Telson (Pl. VII, 13) with three pair on lateral spines and four pair of distal spines, the minute inner spine disappears. Uropod (Pl. VII, 13) and telson more enlarged, setae of both ramus increased; outer ramus with about 2 small setae near the top on outer margin.

Seventh zoea: body length 4.69 mm, carapace length 1.09 mm. Differs from the former stage in the followings: carapace with about 3 small setae under the first rostrum tooth (Pl. I, 7). Chromatophores more prominant than previous stage, especially ventral portion of abdominal somite appears; buds of pleopods more advanced, rudimentary setae only appear at the proximal edge of endopod but still bare (Pl. VII, 2). Antennal flagellum (Pl. II, 7) somewhat longer than the scale, three or four segmented; scale with about 28 setae. Antennule peduncle (Pl. II, 17) beared with more setae around at the articulation of proximal and sub-proximal segments and also mid-portion of proximal peduncle; and about 10 setae on the styloserite. The outer flagellum divided with two branches; inner branch with 4 terminally and 2 aesthetes sub-terminally on the folded appendices; the outer segmented, longer than the inner, with 2 setae at the distal top and another minute seta near the distal top; the outer peduncle flagellum somewhat longer than the inner, with 2 distal setae and a minute seta near the distal portion. First maxilla (Pl. III, 17) more advanced in size; coxa with 7 inwardedly directed spines; basis with 5 teeth and 4 spines. Second maxilla (Pl. III, 27) more advanced; endopod with more setae, about 30 setae all. First maxilliped (Pl. IV, 7) with 9 setae medially directed; basis with 2 median setae near the middle portion on inner margin; exopod with about 5 setae near the proximal portion on the outer side. Second maxilliped (Pl. IV, 17) five-segmented, dactylus, propodus, carpus, merus and aschium, advanced in size, with one more setae on dactylus. Third maxilliped (Pl. IV, 27) with 3 stout setae at the articulation of propodus and carpus; exopod with 4 apical and 4 sub-apical setae.

First and second pereiopod (Pl. V, 7; Pl. V, 17) more or less advanced chelation but not movable chela still, with 4 apical and 6 sub-apical setae in each; second pereiopod longer than the first. Third pereiopod (Pl. VI, 6) with 4 setae on merus. Fourth pereiopod (Pl. VI, 13) endopod with 4 stout setae at the articulation of dactylus and carpus, 3 setae on merus.

Fifth pereiopod (Pl. VI, 22) more advanced, with 6–7 stout setae on propodus inner side. Telson (Pl. VII, 14) more elongated, narrower posteriorly, the proximal edge begins more or less extending back from the mid-portion. Uropod (Pl. VII, 14) more enlarged, all setae of both ramus increased.

Eighth zoea: body length 5.15 mm, carapace length 1.19 mm. Differs from the former in the followings: carapace bears about 3–4 setae and 1 rudimentary tooth under the first rostrum tooth (Pl. I, 8). Pleopods (Pl. VII, 3) advanced almost fully; exopod with rudimentary *appendices internae* except for first pleopod.

Antennal flagellum (Pl. II, 8) longer than the scale, four-segmented, distal top bears with 6 terminal setae; scale with about 29 plumose setae on blade and a slender small single seta near the disto-lateral pointed edge. Antennular peduncle (Pl. II, 18) with more setae around at the articulation of proximal and sub-proximal segments, and also mid-portion of sub-proximal segment; about 12 setae on the stylocerite. Inner peduncle flagellum divided with 2 or 3 segments. First maxilla (Pl. III, 18) coxa with 8 inwardly directed spines. Second maxilla (Pl. III, 28) entire outer edge of endopod almost setose, about 35 setae; three-lobed protopod armed with 3, 4 and 3 plumose setae. First maxilliped (Pl. IV, 8) with about 12 setae on inner margin of basis; exopod with 5–6 setae near the proximal portion on outer side. Second maxilliped (Pl. IV, 18) almost similar to previous stage. Third maxilliped (Pl. IV, 28) with 4 setae on merus.

First and second pereiopod (Pl. V, 8; 18) more advanced; the former smaller than the latter, both chelae movable. Third pereiopod (Pl. VI, 7) with 3 setae at the articulation of propodus and carpus; exopod with 4 apical and 6 subapical setae. Fourth pereiopod (Pl. VI, 4) almost similar to third pereiopod. Fifth pereiopod (Pl. VI, 23) essentially as previous stage in structure, merus with 4 setae. Uropod (Pl. VII, 15) more enlarged, with more setae on margin of both rami; more larger than telson. Telson (Pl. VII, 15) more enlarged and narrower posteriorly, proximal edge extended back from the mid-portion.

Ninth zoea: body length 5.60 mm, carapace length 1.28 mm. Differs from the former stage in the followings: carapace bears about 3 to 5 small setae under the first rostrum tooth (Pl. I, 9), sometimes appear 1 to 4 small teeth front of large rostrum tooth. Pleopods (Pl. VII, 4) advanced with margin setae at both rami, still not setose; exopod with apparent folded *appendices internae* except for first pleopod. Antennal flagellum (Pl. II, 9) with 6 to 9 segments, much longer than scale, 6 distal setae on tip; scale with about 34 setae.

Antennular peduncle (Pl. II, 19) with more setae at the articulation of proximal and subproximal segments, and also mid-portion of subproximal segment; inner branch of outer flagellum with three folded appendices, two of the terminal with aesthetes as before stage but the last folded appendix without aesthetes, the outer branch four-segmented; inner flagellum devided with 3 segments apparently. Mandible (Pl. III, 9) with 7 movable teeth in angle between molar and insicor processes. First maxilla (Pl. II, 19): basis with 6 teeth and 5 spines; coxa with 8 inwardly directed spines. Second maxilla (Pl. III, 29): entire outer edge of endopod setose, about 40 setae, and three-lobed protopod armed with 2, 4 and 3 plumose setae. First maxilliped (Pl. IV, 9): basis with about 16 setae at the inner margin on outer side; endopod with 7–8 setae near the proximal portion on outer side. 2nd to 5th pereiopods (Pl. V, 19; VI, 8, 15, 24): inner ramus with about 4 or 5 setae, the outer with 1 or 2 setae in each; 1st pleopod (Pl. VII, 4a) inner ramus with about 2 setae, the outer without seta and small in size. Telson (Pl. VII, 16): proximal edge more extended back from the mid-portion than previous stage. Uropod (Pl. VII, 16) with more setae on margin of both rami, more enlarged.

Postlarva: body length 5.31, carapace length 1.41 mm. Rostrum somewhat shorter than scale, with 9 dorsal teeth, the first of which is on the carapace directly over the posterior margin of the orbit, and 1 ventral tooth, which is directly beneath the last second tooth; tip of rostrum free of teeth (Pl. I, 10); carapace with antennal and two pair of complete branchiostegal spines (Pl. I, 10). Posterior margins of abdominal pleurae rounded (Pl. I, 10). Anal spine absent.

Table 1. The recognized characters of larvae, *Macrobrachium nipponense* (De Haan) reared in the laboratory under the conditions of water temperature 27.8–28.2°C, salinity 4.56–5.15 ‰ Cl and feeding on *Artemia salina* nauplii. B, biramous; R, rudimentary; U, uniramous; D, degenerative; I, incomplete; Aps, apical setae; Sps, sub-apical setae; Sne, segment of endopod.

Item / Stage	Body length	Recognized characters	Position	Number of appendages							
				Maxilliped			Pereiopod				
				1st	2nd	3rd	1st	2nd	3rd	4th	5th
	mm										
Z 1	2.06	Sessile eyes	Aps	4	4	4	—	—	—	—	—
			Sps	—	—	—	—	—	—	—	—
			Sne	B	3B	3B	R·B	R·B	—	—	—
Z 2	2.27	Stalked eyes	Aps	4	4	4	4	4	—	—	—
			Sps	B	2	2	2	2	—	—	—
			Sne	B	4B	3B	4B	4B	RB	—	RU
Z 3	2.61	A rostral tooth, telson and uropod	Aps	4	4	4	4	4	—	—	—
			Sps	2	2	2	2	2	—	—	—
			Sne	B	4B	4B	4B	4B	RB	—	RU
Z 4	3.07	Two rostral teeth, uropod biramous with setae	Aps	4	4	4	4	4	—	4	—
			Sps	2	2	2	2	2	—	4	—
			Sne	B	4B	4B	4B	4B	RB	4B	6U
Z 5	3.71	Buds of pleopods, antennal flagellum two-segmented	Aps	4	4	4	4B	4B	RB	4	—
			Sps	2	2	2	2	2	—	2	—
			Sne	B	4B	4B	4B	4B	1B	4B	6U
Z 6	4.24	Pleopods biramous and rudimentary; rudimental chelae of pereiopods	Aps	4	4	4	4	4	4	4	—
			Sps	2	2	2	2	2	2	2	—
			Sne	B	4B	4B	4B	4B	4B	4B	6U·R
Z 7	4,69	Pleopods biramous, bare; antennal flagellum 3 or 4-segmented	Aps	4	4	4	4	4	4	4	—
			Sps	2	2	4	6	6	2	2	—
			Sne	B	5B	4B	4B	4B	4B	4B	6B
Z 8	5.15	Movable chelae, telson convex posteriorly	Aps	4	4	4	4	4	4	4	—
			Sps	2	2	4	6	6	6	6	—
			Sne	5B	4B	4B	4B	4B	4B	4B	6B
Z 9	5.60	Pleopods with setae, antennal flagellum 7–9-segmented, antennular inner flagellum 3-segmented	Aps	4	4	4	4	4	4	4	—
			Sps	2	2	4	6	6	6	6	—
			Sne	B	5B	4B	4B	4B	4B	4B	6B
PL	5.31	Behaviors of swimming and locomotion as adult.	Aps	4	4	4	—	—	—	—	—
			Sps	2	2	4	—	—	—	—	—
			Sne	B	5B	3B	3B·D	5B·D	5B·D	5B·D	6B·D

Telson (Pl. VII, 17) with a pair of large single spines, a pair of single and another pair of plumose setae terminally; two pair of lateral spines moved dorsally. Antennal flagellum with about 28 to 34 segments; length of antennular scale about four times of its width, outer margin slightly concaved; anterior end of spine projects free of blade and slightly shorter (Pl. II, 10). Antennal flagellum over half of total length. Antennular peduncle (Pl. II, 10) of

3 segments; stylocerite less than the half length of the basal segment of peduncle; antero-lateral spines of basal segment exceeding anterior margin of segment; inner side of peduncle with about 10 setae; basal segment containing a statocyst and a short ventral tooth. Inner antennular flagellum simple and with about 8 segments; outer branch of outer flagellum with about 8 segments, the inner branch with 3 folded appendices bearing 4, 2 and 0 aesthetes, from distal to proximal folded appendices. Mandible (Pl. III, 10) strong, incisor process stouter than that of zoea larva; teeth of molar process large, forming a triangular surface, without movable teeth in angle. Basal portion of first maxilla (Pl. III, 20) bilobed, each lobe bearing on its inner surface numerous coarse setae; endopod palp-like. Basal portion of second maxilla bilobed, each lobe bearing on its inner surface with coarse setae (Pl. III, 30); endopod unsegmented, bare; exopod setose around margin. Basal portion of first maxilliped (Pl. IV, 10) large, bilobed, the lobes with coarse setae directed inwardly; endopod reduced with 2 distal setae; exopod with about 14 setae at the proximal portion of basis, and 4 apical and 2 sub-apical setae; epipod large and bilobed completely. Second maxilliped (Pl. IV, 20) with five-segmented endopod, ultimate and penultimate segments wider than long, armed with coarse spines; exopod with 4 apical and 2 sub-apical setae; epipod tiny, biramous. Third maxilliped (Pl. IV, 30) with three-segmented, endopod coarsely setose throughout each segment; exopod reduced, with 4 apical and 4 sub-apical setae; epipod tiny, and bilobed. First and second pereiopod (Pl. V, 10, 20) chelate, first pereiopod shorter than second; both of exopod rudimentary. Cutting edge of chelae neither serrations nor teeth, carpus shorter than palm. Third, fourth and fifth pereiopod with strong claw; endopods with coarse setae in each segment; exopods rudimentary if present, or lacking; commonly fifth pereiopod without exopod (Pl. VI, 25).

Uropodal exopod (Pl. VII, 17) setose along outer margin with a tooth and a movable spine in the disto-lateral corner (Pl. VII, 17a), numerous setae around the tip and on inner edge; endopod setose.

Table 2. The growth of larvae, *Macrobrachium nipponense* (De Haan) in the laboratory. Rearing conditions: water temperature 27.8–28.2°C, salinity 4.56–5.15 ‰ Cl, feeding on *Artemia salina* nauplii. m, mean; sd, standard deviation.

Item / Stage	Inter-molt period	Carapace length		Body length		No. of specimen
		m	sd	m	sd	
	days		mm		mm	
Z 1	1–2	0. 53	0. 005	2. 06	0. 027	11
Z 2	3–3	0. 53	0. 007	2. 27	0. 027	10
Z 3	3–5	0. 58	0. 017	2. 61	0. 062	11
Z 4	5–7	0. 70	0. 072	3. 07	0. 074	13
Z 5	6–9	0. 88	0. 013	3. 71	0. 071	16
Z 6	8–12	0. 98	0. 026	4. 24	0. 154	22
Z 7	11–15	1. . 9	0. 017	4. 69	0. 103	22
Z 8	13–17	1. 19	0. 037	5. 15	0. 151	23
Z 9	15–20	1. 28	0. 047	5. 60	0. 218	25
PL	18–23	1. 41	0. 077	5. 31	0. 344	30

The distinctive chromatophores on all body surface which characterized the zoea larvae are concentrated, and transparent white in the post-larva.

The recognized characters of each stage are summerized in Table 1. The larva of *Macrobrachium nipponense* metamorphoses a day after hatching to second zoea and from three zoea spends regularly molting period, three or four days per a molting.

Larval growth of body length and carapace length are shown in Table 2 and Fig. 1. Body

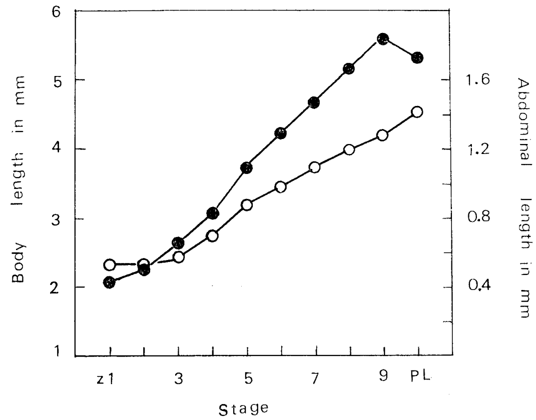

Fig. 1. The growth of larvae, *Macrobrachium nipponense* in the laboratory. Black circles, body length; white circles, carapace length.

length in each stage from the first through ninth zoea to postlarva is respectively as follows: 2.06 ±0.027, 2.27±0.027, 2.61±0.062, 3.07±0.074, 3.71±0.071, 4.24±0.154, 4.69±0.103, 5.15±0.151, 5.60±0.218 and 5.31±0.344 mm.

Body length, especially abdominal length becomes short when zoea larvae molt to postlarvae. Standard deviations of body length from the first to fifth zoea are less than 0.1 mm, while the values of the sixth to postlarva, more than 0.1 mm. It is found that the varying of body length in the larvae of earlier stage till fifth zoea almost does not occur, but from sixth zoea is distinct.

4. Discussion

The larva of *Macrobrachium nipponense*, mentioned above in the result, metamorphoses a day from hatching to second zoea under the present laboratory conditions and third zoea to the ninth spends regularly molting period, three or four days. This species molts to postlarva through nine zoeal stages, but *Macrobrachium rosenbergi*, through eleven zoeal stages (UNO and KWON, 1969).

The differences of morphological characters of appendages, distribution of chromatophores and varying of body length on each early developmental larvae are slight, in general, and the similarities are great between *Macrobrachium nipponense* and *M. rosenbergi*. The distinct differences of both species are of larval size, structure of mandible and first maxilla, and distribution of chromatophores of third ventro-abdominal somite of newly hatched larva. The mandible incisor process of this species is less advanced than that of *Macrobrachium rosenbergi*; first maxilla coxa is formed with four or five tiny spines covering with thin cuticle membrane. Distributed chromatophores of both species as shown in Fig. 2. Chromatophores of *M. nipponense* are two contractive outer and a expansive inner located on the third somite as compared with *M. rosenbergi*, two expansive outer and a contractive inner. The larvae of *M. nipponense* from the first to eighth zoea are larger than those of *M. rosenbergi* in body length, while the ninth zoea and postlarva are distinctly less than *M. rosenbergi*.

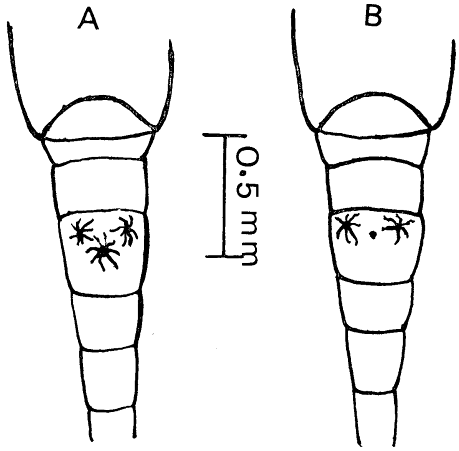

Fig. 2. Distributive differences of chromatophores of newly hatched larva on the third ventro-abdominal somite between *Macrobrachium nipponense* (A) and *Macrobrachium rosenbergi* (B).

It is similar phenomenon which we have reported on *M. rosenbergi* that body length of this species becomes short when zoea larva molts to postlarva.

5. Summary

1. *Macrobrachium nipponense* of ovigorous female prawns are breeded in the laboratory under the conditions of temperature 27.8–28.2°C, salinity 4.56–5.15 ‰ Cl and flow of water 0.8 *l*/min.

2. Eggs are slightly oval in shape more than that of *Macrobrachium rosenbergi*, measuring from 0.54×0.67 mm change to 0.59×0.92 mm on the average; being light greenish gray primitively in color and changed to light gray owing to advance of development; body length of newly hatched zoea larvae is 2.06 mm and first postlarvae is 5.31 mm on the average. This species is also decreased on body length when ninth zoea larvae were metamorphosed to first postlarvae as *Macrobrachium rosenbergi* did.

3. Under the laboratory conditions, larvae go through nine zoeal stages to first postlarvae in 20 days approximately, while fastest development from eggs to postlarvae occurred in 18 days. Zoeal stages are described and figured.

4. The differences of morphological characters of appendages, distribution of chromatophores and variance of body length on each early de-

velopmental larvae are slight, in general, and the similarities are great between *Macrobrachium nipponense* and *Macrobrachium rosenbergi*, while some of differences of both species are as followings: 1) Incisor process of mandible is less advanced than that of *Macrobrachium rosenbergi*; this species forms incisor process with incomplete two teeth at tip, molar portion without fine toothed cutting edge and a movable tooth in angle between molar portion and incisor process. 2) Coxa of first maxilla of this species is formed with four or five tiny spines covering with thin cuticle membrane as compared with *Macrobrachium rosenbergi*, coxa with four inwardly directed spines. 3) This species is distributed with two contractive outer and one expansive inner chromatophores located on dorso-ventral portion of third abdominal somite when just hatch out.

5. Variation of body length occurs in the same zoeal stage, especially from sixth zoeal stage apparently.

References

HOLTHUIS, L. B. (1950): The *palaemonidae* collected by the Siboga and Snellius Expeditions with remarks on other species. I. Sub family *Palaemoninae*. In the Decapoda of the Siboga Expedition. Patt X. Siboga Exped. Mon. 39a 91-268.

ICHO, H. (1914): Japanese fresh water *Palaemonid* prawns and their lavae (in Japanese). Dobutsugaku Zasshi, **26**, 183-187.

KUBO, I. (1940): On the taxisonomical studies of Japanese *Palaemonidae*. I. *Palaemon* (in Japanese). Jour. Imp. Fish. Inst., **34**(1), 5-26.

KUBO, I. (1949): Ecological studies on the Japanese fresh-water shrimp, *Palaemon nipponensis*. 1. Seasonal migration and monthly size-composition with special reference to the growth and age. Bull. Jap. Soc. Sci. Fish., **15**(3), 125-130.

KUBO, I. (1950): Ecological studies on the Japanese fresh-water shrimp, *Palaemon nipponensis*. 2. Localization found on the population of the shrimp of the Lake Kasumigaura (in Japanese). Bull. Jap. Soc. Sci. Fish., **15**(10), 561-566.

KWON, C. S. and Y. UNO (1968): The larval development of *Palaemon modestus* (Heller) in the laboratory. La mer, **6**(4), 263-278.

LEWIS, J. B. and J. WARD (1965): Developmental stages of the *Palaemonid* shrimp, *Macrobrachium carcinus* (Linnaeus, 1788). Crustaceana, **9**, 137-148.

LING, S. W. (1962): Studies on the rearing of larvae and juveniles and culturing of adults of *Macrobrachium rosenbergii* (De Man). Indo-Pacific Fish. Counc., Curr. Affairs Bull., **35**, 1-11.

LING, S. W. and A. B. O. MERICAN (1961): Notes on the life and habits of the adult and larva stages of *Macrobrachium rosenbergii* (De Man). Proc. Indo-Pacific Counc., **9**(2): 55-60.

UNO, Y. and C. S. KWON (1969): Larval development of *Macrobrachium rosenbergi* (De Man) reared in the laboratory. Jour. Tokyo Univ. Fish., **55**(2), 179-190, Pl. 12.

テナガエビ *Macrobrachium nipponense* (De Haan) 幼生の発生について

権　晋　洙　　宇　野　　寛

要旨: 日本の淡水産テナガエビ科の中で，産業的に最も重要なテナガエビの幼生を水槽中で飼育した。本種幼生は *Artemia salina* の幼生を投与し，水温 27.8-28.2°C，塩分量 4.56-5.15‰ Cl の条件下で飼育した場合，九つの zoea 期を経て postlarva に変態する。幼生各期の形態を述べ図示するとともに，世界最大の淡水エビの一つであるオニテナガエビ，*Macrobrachium rosenbergi* (De Man) のそれと比較検討した。両種の幼生は大きさ，mandible と 1st maxilla の構造および第3腹節の色素によって区別することができる。

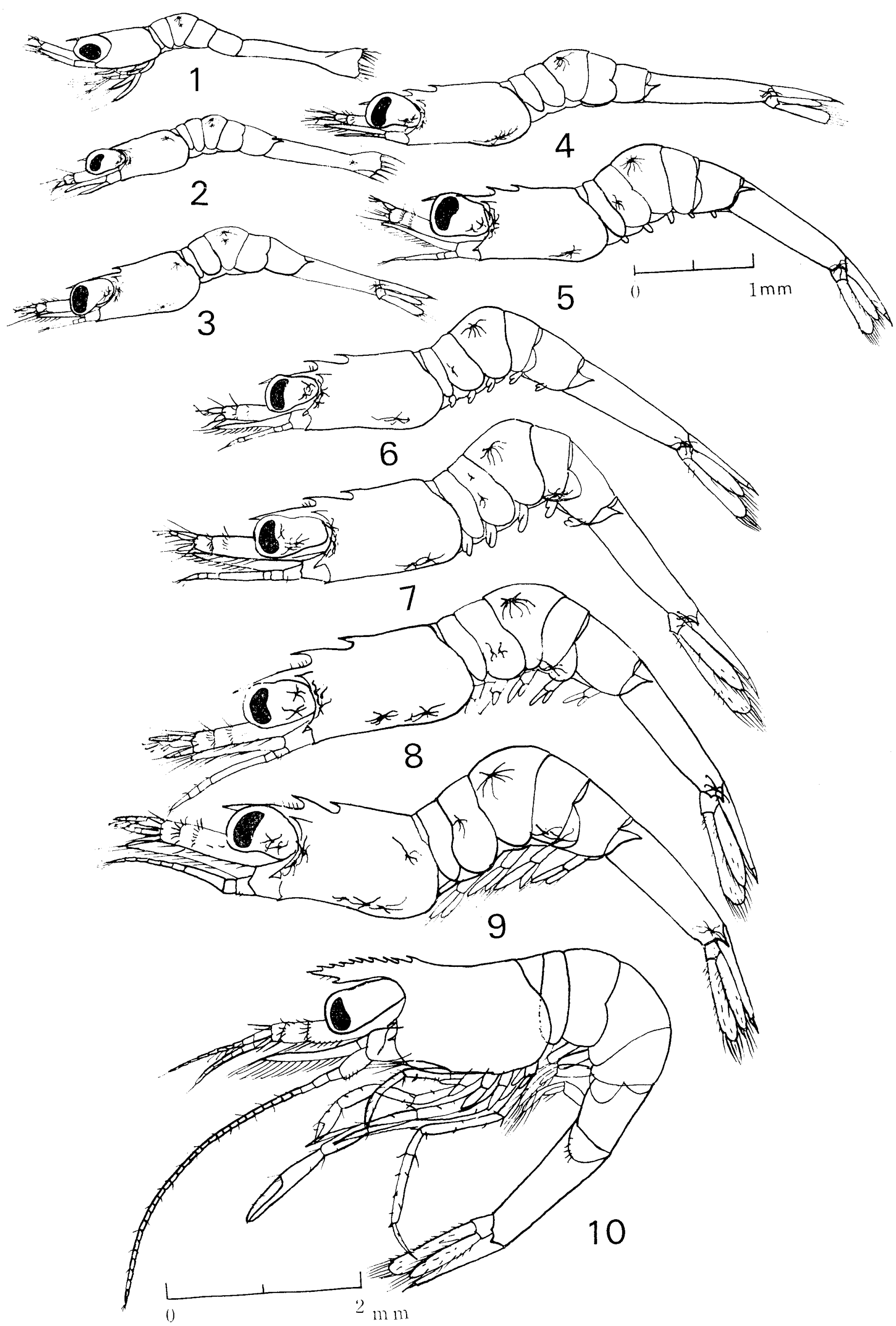

Plate I. *Macrobrachium nipponense* (De Haan), lateral view. 1-9, zoea I-IX; 10, postlarva.

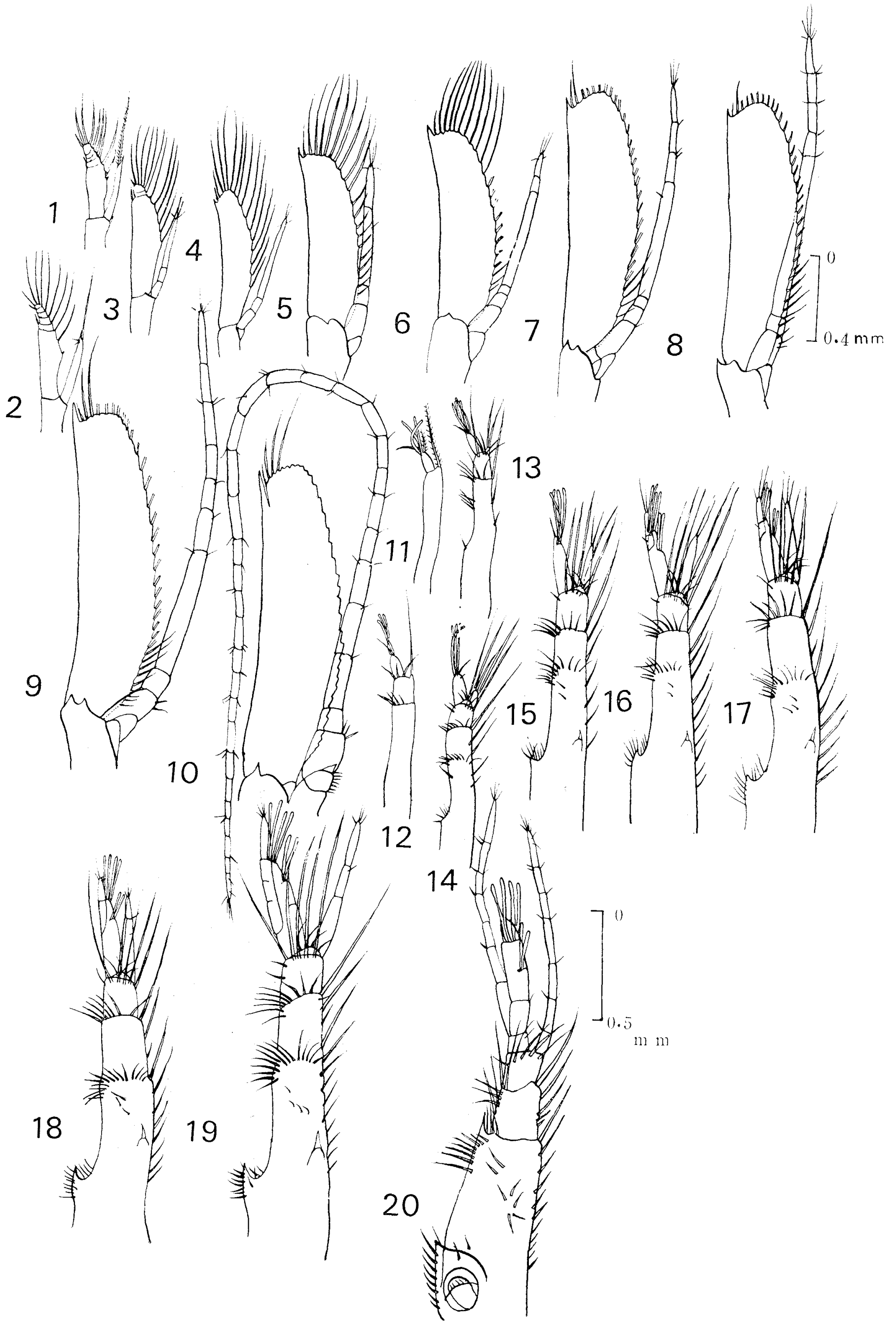

Plate II. *Macrobrachium nipponense* (De Haan). Antenna: 1–9, zoea I–IX; 10, postlarva. Antennule: 11–19, zoea I–IX; 20, postlarva.

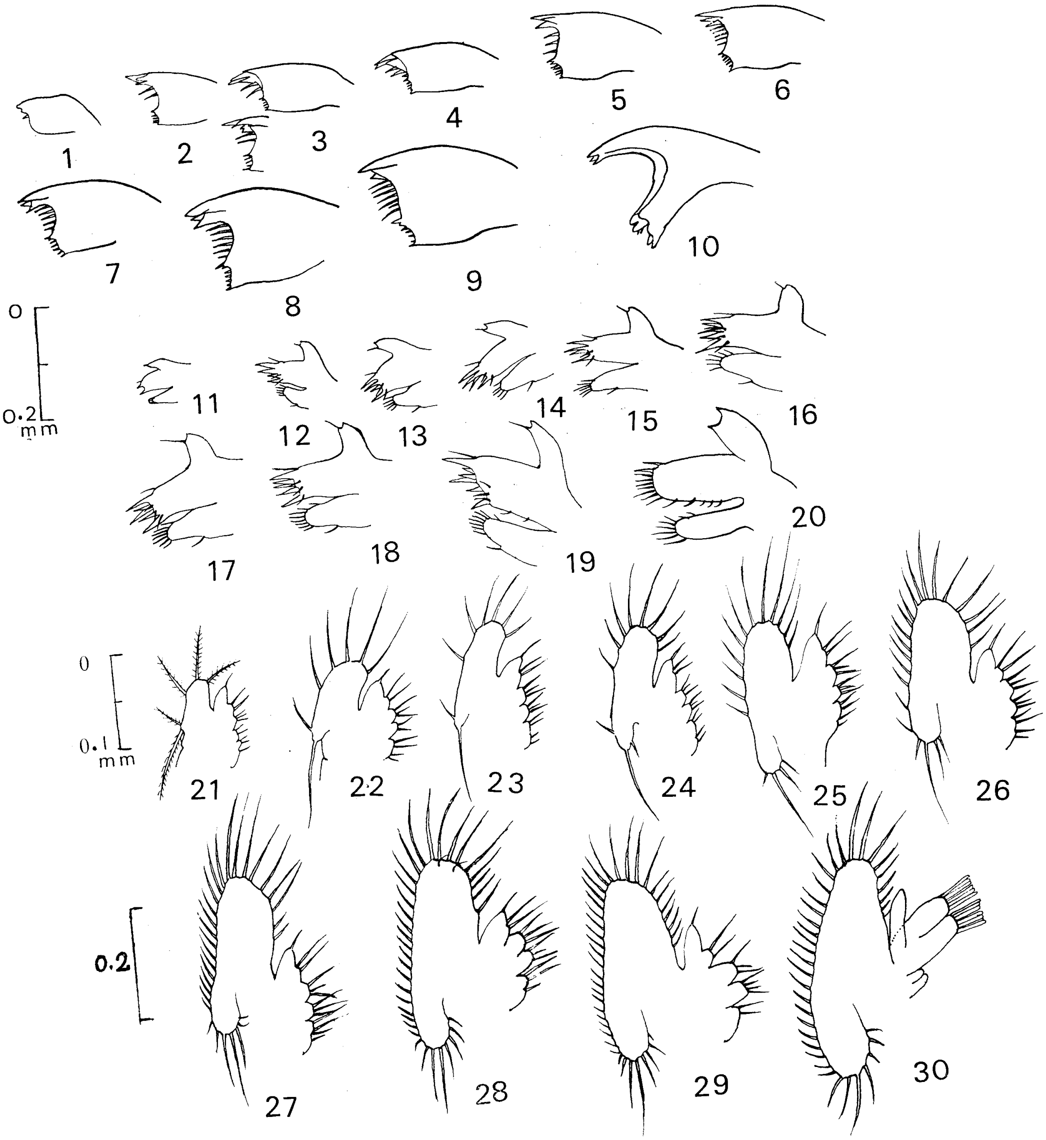

Plate III. *Macrobrachium nipponense* (De Haan). Mandible: 1–9, zoea I–IX; 10, postlarva. First maxilla: 11–19 zoea I–IX; 20, postlarva. Second maxilla: 21–29, zoea I–IX; 30, postlarva.

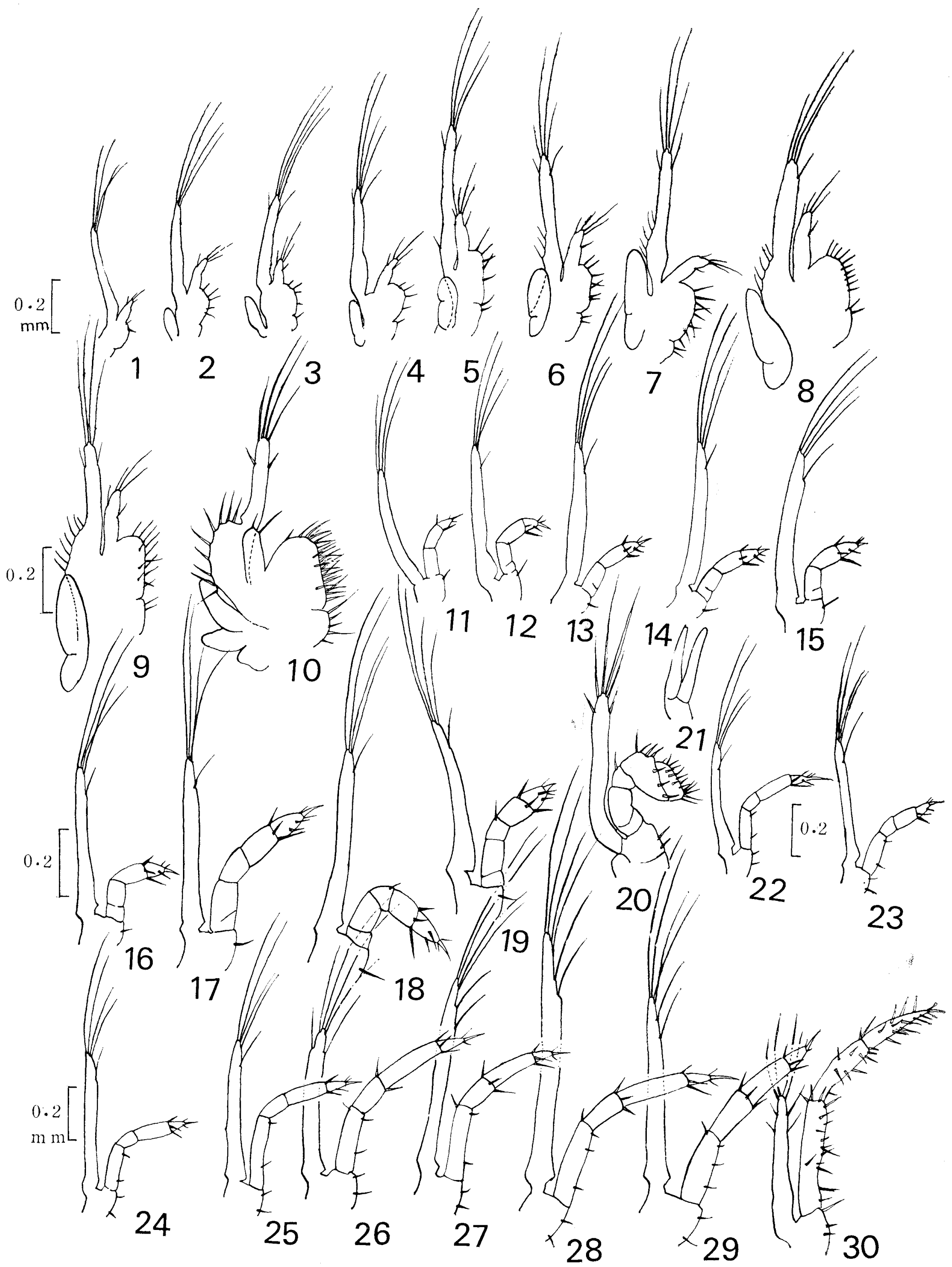

Plate IV. *Macrobrachium nipponense* (De Haan). First maxilliped: 1-9, zoea I-IX; 10, postlarva. Second maxilliped: 11-19, zoea I-IX; 20, postlarva. Third maxilliped: 21-29, zoea I-IX; 30, postlarva.

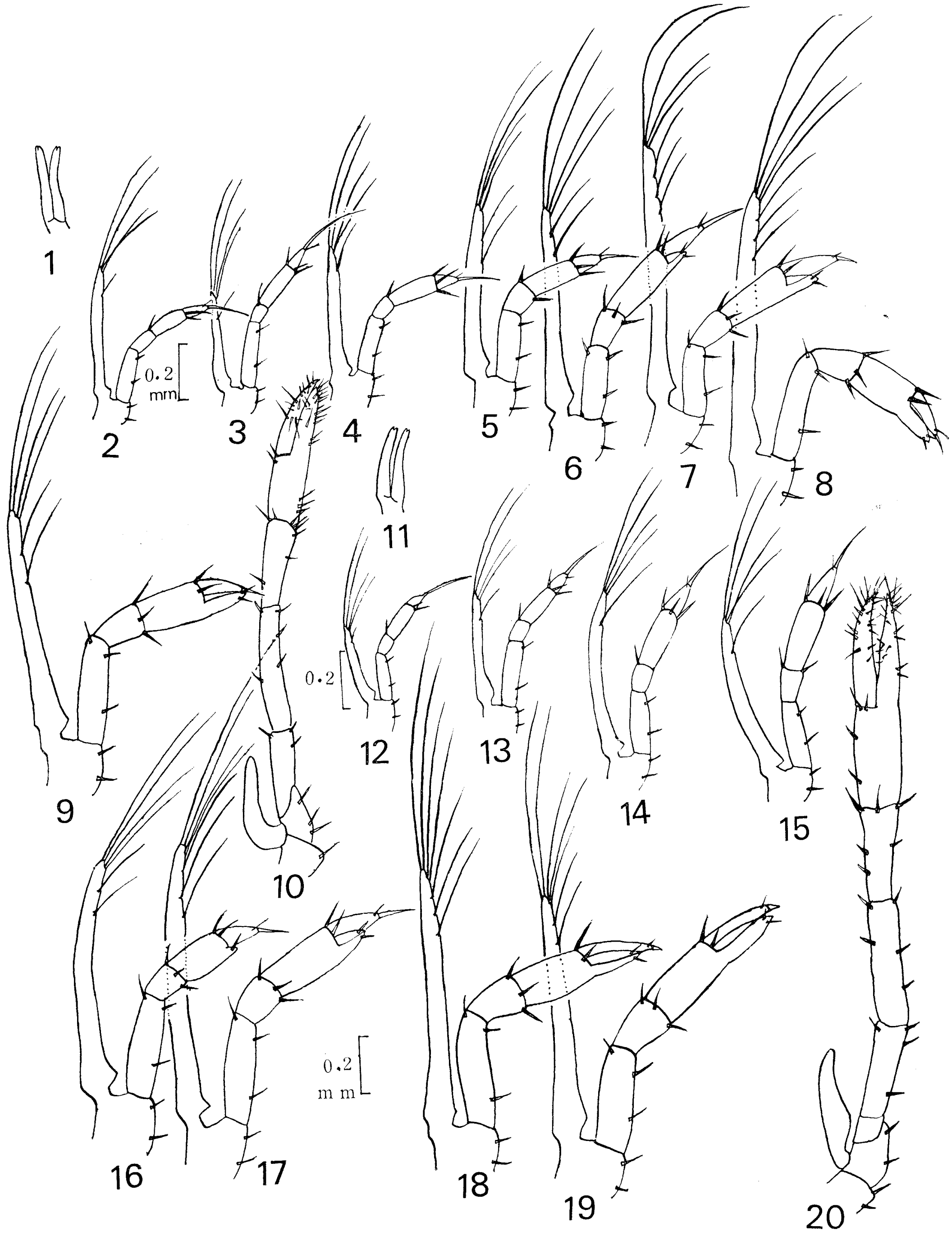

Plate V. *Macrobrachium nipponense* (De Haan). First pereiopod: 1–9, zoea I–IX; 10, postlarva. Second pereiopod: 11–19, zoea I–IX; 20, postlarva.

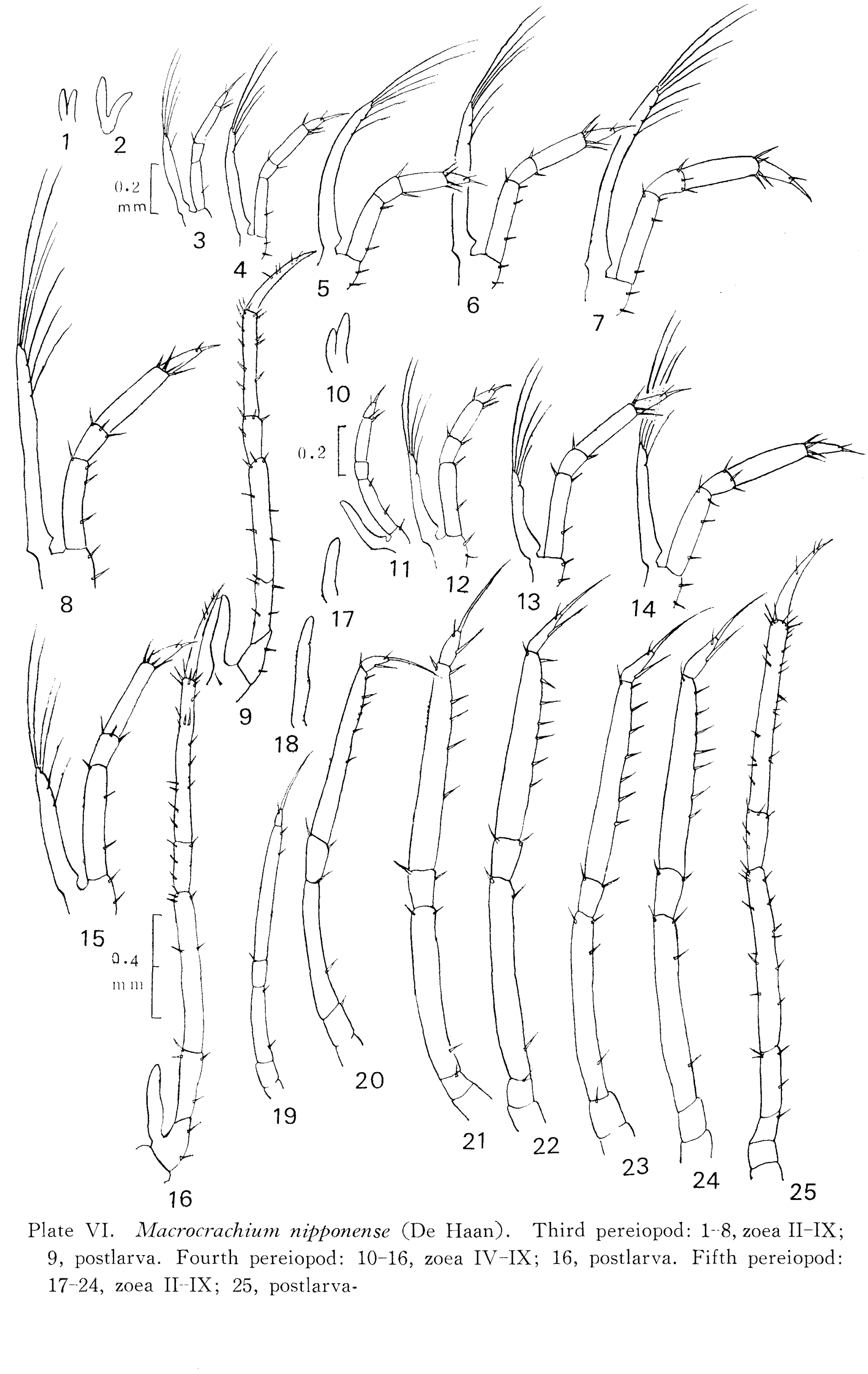

Plate VI. *Macrocrachium nipponense* (De Haan). Third pereiopod: 1–8, zoea II–IX; 9, postlarva. Fourth pereiopod: 10–16, zoea IV–IX; 16, postlarva. Fifth pereiopod: 17–24, zoea II–IX; 25, postlarva.

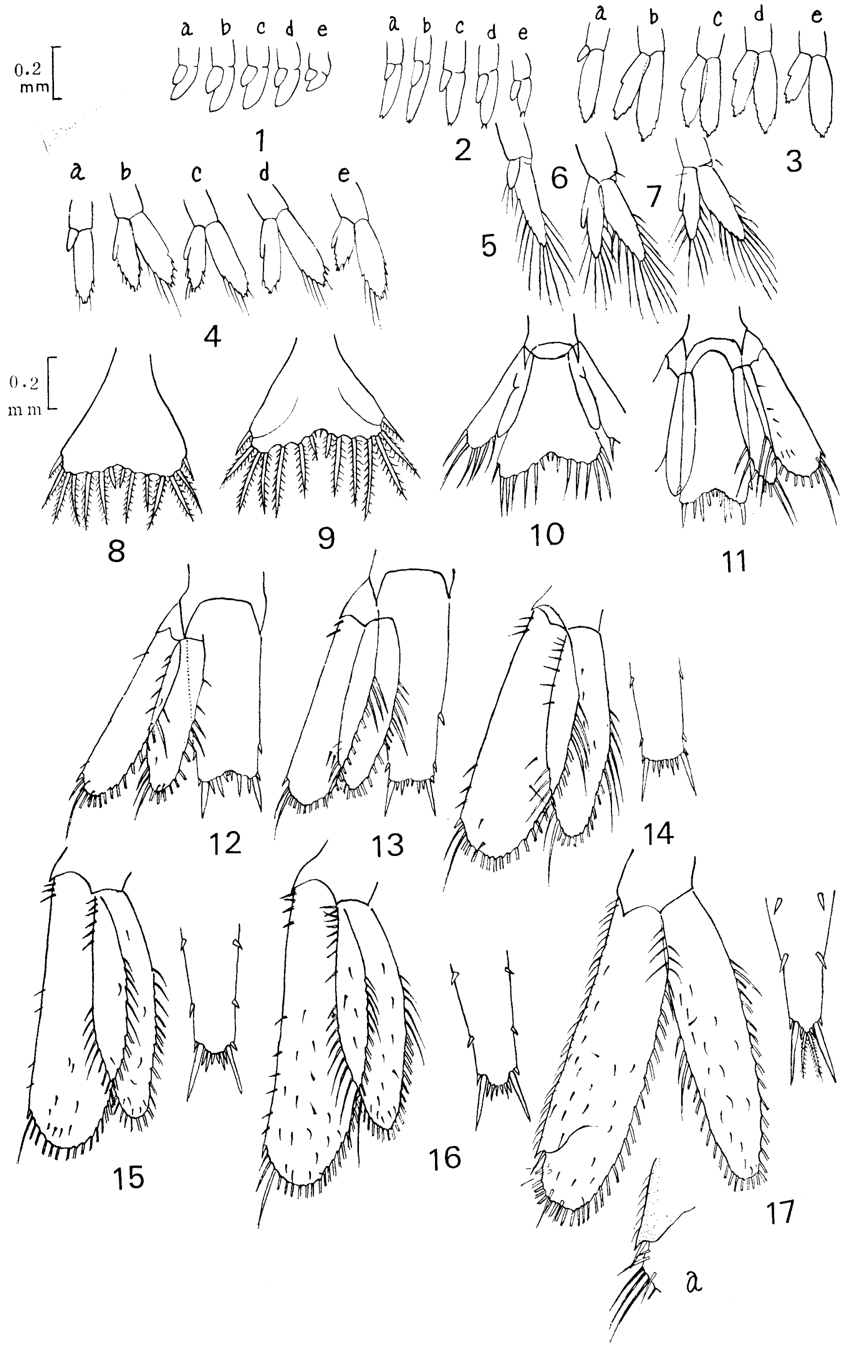

Plate VII. *Macrobrachium nipponense* (De Haan). Pleopod: 1-4, zoea VI-VIII; a-e, 1st-5th pleopod. Postlarva pleopod: 5-7, 1st, 3rd and 5th pleopod. Telson and uropod: 8-16, zoea I-IX; 17, postlarva.

資　　料

ソビエトにおける海洋学書の出版の近況*

Situation actuelle de la publication océanographique en Russie

吉　村　広　三**

ソビエトの海洋学界の定期刊行物としては，科学アカデミー海洋研究所の「海洋研究所紀要」(Труды Института Океанология) を始め，水理気象局国立海洋研究所，ウクライナ科学アカデミー海洋物理研究所などの出版物が日本の関係機関にしばしば送られてきているほか，ロシヤ語書の輸入商社によっても取り扱われているため，比較的に接する機会が多い。しかし，単行本についてはその出版状況がよく解らなかったため，ナウカ社のカタログを手がかりにして1966年以後の海洋学書の近況を調べてみた。

ソビエトの海洋学専門書はこの数年間，毎年10冊程度出版されており，そのうち9割までがソ連の人の新らしい著述で，残りは殆んど英文のロシヤ語訳となっていた。

また，出版所からみると，モスクワの科学アカデミー出版所「ナウカ」(Наука) からの出版数が圧倒的に多く，約半分を占め，残りがレニングラードの水理気象出版所，モスクワの「小さな科学の出版所」，モスクワ大学出版所などの出版となっていた。

それらの単行本のうち，われわれにとって特に参考になると思われるものを以下に列記する。

まず目につくものに科学アカデミー海洋研究所で編集している太平洋シリーズものがある。これは一般海洋学のベ・ゲ・コルト博士が編集長になり，化学のブルエビッチ，海洋生物のゼンケビッチ，底質のベズルコフ，沿岸海洋のゼンコビッチ博士ら8名の学者を編集陣にして刊行中のもので，現在までに 1.「太平洋上の気象条件」(Метеорологические условия над Тихим океаном) 2.「太平洋の水理学」(Гидрология Тихого океана) 3.「太平洋の化学」(Химия Тихого океана) 4.「太平洋の海岸」(Берега Тихого океана) 6.「太平洋の水成岩の形成」2分冊 (Осадкообразование в Тихого океана) が刊行されており，5.「太平洋底の構造と地殻変動」(Геоморфология и тектоника дна Тихого океана) と 7.「太平洋の生物学」(Бпология Тихого океана) が未刊となっている。編集の形態は編集委員がそれぞれの専門に従って責任者となり，各分野の責任者の下に科学アカデミー海洋研究所の第一線の研究者がついて，さらに分けられたいくつかの専攻部門を分担執筆する形をとっており，太平洋地域各国（ソ，米，日，カナダ，オーストラリヤなど）の生の資料を網羅し，分布図などをまとめている点が特徴的である。

次に目につくものとしては海洋調査法が2冊出ていることで，その中の1冊「海洋の水理調査についての手引き」(Руководство по гидрологическим работам в океанах и морах，エリ・エス・ボリシャンスキイ，1967年，水理気象出版所）は500頁ほどで，さしずめソビエトの海洋観測指針とみなせる。

海洋物理学の分野の発行書では，国際地球観測年およびそれ以後の資料に基づき，北大西洋の海の波を季節別に取り扱ったり，波の発達や風との関連の解明を試みている「大西洋北部の波高」(Высоты волн севернсй части Атлантического океана，カ・イ・カシン，1966年，ナウカ出版所）と波の理論を扱った「海の波の力学」(Динамика морских волн，コノンコバ，1968年，モスクワ大学出版所）が波浪の部門で出されている。また，海流などの部門では，海洋，地球物理，地理，水産，海運などの技術者，研究者を対象にして，北大西洋の海流系やその季節変動，溶在酸素極少層の形成などを記述した「大西洋の水理学」(Динамика вод Атлантического океана，科学アカデミー海洋研究所，1966年，ナウカ出版所）や，海水の鉛直面での力学を扱った冊子「大洋における海水の鉛直運動」(Вертикалиные движения вод в океане，カ・ア・チェコチロ，1966年，ナウカ出版所）があり，後者は北西太平洋の資料を用いている。さらに日本付近の海域を扱ったものに「ベーリング海の水塊と海流」(Течения и водные массы Берингова Моря，ベ・エス・アルセニエフ，1967年，ナウカ出版所）と「オホーツク海の水塊」Водные Массы Охотского Моря，カ・ベ・マロシュキン，1966年，ナウカ出版所）の2冊子があり，他の部門では「海洋における電磁現象」(Электромагнитные явления в Моря，論文集，1968年，小さな科学の出版所）が出されている。

* 1969年8月4日受理

** Hirozo YOSHIMURA 気象庁海洋課 Oceanographical Section, Japan Meteorological Agency

海洋化学の分野の出版数は少ない。しかし特に記すべきものに，科学アカデミー会員，分析化学・地球化学研究所長のア・ペ・ビノグラドフ教授による「海洋地球化学概論」(Введение в геохимию океана, 1967 年, ナウカ出版所) が出されていることで，地球の宇宙塵形成説の基礎の上に立って海洋の生成の問題点を取り上げているほか，各論の部分では海水中の塩類を始め，溶在ガス，懸濁物質，有機物，微量元素，堆積物など，くまなく触れられている点が特徴的である。A 5 判 212 頁の本ではあるが，引用文献はソ，日，米などを主にして 488 編に及んでいる。この分野でもう一つ特に述べたいことは，化学の三宅泰雄先生の著，“Elements of Geochemistry” (1965 年, 丸善) が近くロシア語訳となってモスクワで出版されるという予告があったことで，日本のわれわれのためにも大変嬉しいニュースである。

海洋地質学の分野では科学アカデミー会員で「構造地質学」の大著でよく知られているベロウソフ教授による「地殻と海洋上部マントル」(Земная кора и верхняя мантия океанов, 1968 年, ナウカ出版所) がある。また，教育的な専門書としては，モスクワ大学海洋学教室のレオンチェフ博士の「海底」(Дно океана, 1968 年, 思索出版所) が出版されており，海洋地質学，海底物理学における国際地球観測年以後の豊富な成果を手際よく盛り込んだ好著と言える。その他，ビーチャシ号で来日したこともあるリシィツィン博士の「ベーリング海における現在の堆積過程」(Процессы современного осадкообразования в беринговом море, 1966 年, ナウカ出版所) もベロウソフ教授の監修を経ており，ベーリング海底の研究上重要な参考書とみられる。堆積に関連して，「太平洋西部の深海堆積物の絶対年代の測定と層位学」(Стратиграфия и абсолютный возраст глубоководных осадков западной части Тихого океана, エ・ア・ラマンケビッチ，ペ・エリ・ベズルコフ他, 1966年, ナウカ出版所) が出版されており，第四紀の気候変動やそのヨーロッパとの対比，生物の残がいや土砂の堆積に対する気候変動の影響などが述べられている。

放射能調査に関しては，「世界の海洋の放射能汚染調査」(Исследование радиоактивной загрязненности Мирового океана, 科学アカデミー海洋研究所, 1966 年, ナウカ出版所) があり，前掲，太平洋シリーズの「太平洋の水理学」と共に米国で英訳出版されている。

海洋生物学の分野では「海洋性窒素固定菌の生物学」(Биология морских азотфиксаторов, エリ・エン・プシェニン, 1966 年) なる著がある。また論文の集録で「太平洋のプランクトン」(Пранктон тихого океана, 1968 年, ナウカ出版所) も同じく 200 頁ぐらいの本である。そのほか，「世界の海洋の超深海性動物相 (Фауна ультраабиссали Мирового океана, ゲ・エム・ベリヤエフ, 1966 年, ナウカ出版所)，「北太平洋とソ連邦の水管類」(Сифонофоры морей СССР и северной части Тихого океана, エス・デ・ステパニャンツ, 1968 年, ナウカ出版所) などの書名を見ることができる。

本来の理学からははずれるが，ソビエトの北極航路を扱ったものに「北方航路発見開拓史」(История открытия и освоения Северного морского пути, 1967 年に第 4 巻が刊行，エム・イ・ベーロフ，水理気象出版所) があり，同じ型類に属するものとして「ソビエト海洋調査史」(Советские океанографические экспелиция, カ・カ・デェルューギン, 1967 年, 水理気象出版所) がある。

なお，一般向けの教養書として「海洋の秘密」(Тайны океана, エン・エン・ゴルスキイ, 1968 年, ナウカ出版所)，「地表における循環水およびその量，起源に関する認識の発展」(Развитие знаний о происхождении, количестве и круговороте воды на земле, イ・ア・フェドセエエフ, 1967 年, ナウカ出版所)，「南極海でアクアラングと」(С аквалангом в Антарктиде, エム・ベ・プロップ, 1968 年, 水理気象出版所) などがあるが，程度はいずれもかなり高い。

例をあげればゴルスキイの著書の中には世界の潮汐発電所のプランの一覧表も記されていたり，フェドセエエフの著書の中には古代の地図が 6 図も入っているという具合である。

以上で極くおおざっぱな概観を述べたつもりだが，直接に実物を手にすることのできた本の方が少なかったため，内容紹介の多々至らなかった点は御容赦頂きたい。

録　　事

昭和44年9月30日，理化学研究所において幹事会が開かれた.

来年 4月25日～29日，フランスの ASTEO (Association Scientific et Technique pour l'Exploitation des Océans) の主催で国際海洋開発会議が開催される予定であるが，本会議に出席並びにヨーロッパ海洋開発事情視察団の編成を本学会主催で行なうことになった。

なお，来年は本学会の創立10周年にあたるので，10周年記念事業を行なうことにし，次の諸氏に10周年記念事業委員会の委員をお願いすることにした。

加賀美英雄，川原田　裕，大柴五八郎，杉浦吉雄，高木和徳，高野健三，冨永政英，山中鷹之助

(abc 順，敬称略)

2. 昭和44年11月4日，理化学研究所において，第1回10周年記念事業委員会を開き，記念事業について検討した。互選の結果，冨永幹事が委員長に選ばれた。

3. 昭和44年11月13日，理化学研究所において編集委員会が開かれ，第7巻第4号の編集を行なった。

4. 下記の諸氏が入会された。

正会員

氏　名	所　属	紹介者
長田　幸雄	鹿島建設技術研	佐々木忠義
田口　　正	東海大・海洋	〃
関　　邦博	淀川精機 KK	〃
宮田　元靖		永田　　豊

賛助会員

(社)日本能率協会	中島清一	佐々木忠義

5. 会員の住所，所属の変更。

氏　名	新住所又は新所属
飯高勇之助	近畿大・農・水産学科
栗田　俊行	清水市北矢部 1-3-11 竹栄荘 204
青木　　洋	埼玉県入間郡福岡町西 2-5-25
川村文三郎	海上保安庁水路部マラッカ海峡調査室
松井　孝允	東海大・海洋学部
古橋　賢造	舞鶴海洋気象台海洋課
小出　五郎	札幌市真駒内曙町あけぼの団地 20-509
沼田　貞三	千代田区内神田 1-5-9 丸山ビル (社)海中開発技術協会
安田　秀明	愛知県木曽川町松山
山本　裕彦	府中市小柳町 3-7
棚橋　善克	函館市弥生町 2-33 函館市立病院
工藤　勝宏	大分県南海部郡上浦町津井 大分県水産試験場
極東貿易KK	東京都千代田区大手町 2-2-1 新大手町ビル
三菱重工KK	東京都千代田区丸の内 2-5-1

6. 交換および寄贈刊行物。

1) 逐次刊行物目録(国会図書館)，昭和42年度.
2) 研究実用化報告(日本電電・電通研)，**18**(9～11)，1969.
3) 湖沼研概報(滋賀大)，昭和43年度.
4) 海洋機器開発，9，1969.
5) 日本航海学会誌，41 号，1969.
6) 広島大水畜産学部紀要，**8**(1)，1969.
7) 農業土木試技報，D 5，6 号，F 3 号，1969.
8) 農業土木試報告，No. 7，1969.
9) 研究論文集（理研)，1968.
10) 港湾技研資料，No. 81～99，1969.
11) 港湾技研研究報告，**8**(3)，1969.
12) 港湾技研年報，昭和44年度.
13) 科学博物館研究報告，**12**(**3**)，1969.
14) 科学博物館専報，No. 2，1969.
15) 日本プランクトン学会報，**16**(1)，1969.
16) 航海，30号，1969.
17) ウオーターレビュー（工業開発研)，**1**(21～26)，1969.
18) 海洋産業研究会報，No. 2，1969.
19) 神奈川県立博物館研究報告，**1**(3).
20) 日仏生物学会誌，**14**(2)，1969.
21) Science et Pêche, N° 179, 180, 183, 1969.
22) Revue des Travaux de l'Inst. des Pêches Maritimes, Tome XXXII, Fasc. 3, 4; Tome XXXIII, Fasc. 3, 1969.
23) Cahiers Océanogr., Tome N° 3, Années 1964～1968; XXI^{e} Année N° 8, 1969.

お　知　ら　せ

第2回　黒潮共同調査（CSK）シンポジウム

黒潮共同調査の成果をまとめるためのシンポジウムが開催される。このシンポジウムは，1968年にホノルルで開催された第1回シンポジウムのフオローアップとしてのものである。

時:　昭和45年9月28日～10月1日

所:　東　　京

参加希望者は，昭和45年3月15日までにコンビーナー宛に所定の様式にしたがって登録すること。

連絡先:　〒100 東京都千代田区霞ケ関 3-2-2
日本ユネスコ国内委員会
第2回黒潮共同調査シンポジウム
コンビーナー　菅原　健

お　知　ら　せ

このたび，フランスの A. S. T. E. F. (Association pour l'organisation des Stages en France) より当学会会長宛に下記のような連絡を受けましたのでお知らせいたします。

記

来る1971年に海中探査及び海中工事に関するセミナーを企画しております。海中工事に関しては，広義に解しており，深い河川や湖における水中の諸活動も含まれるものと考えます。

多数のフランスの会社は，この種の技術，すなわち多種の水中土木工事（岸壁，橋脚，沈没船，坐礁船の離礁等），特に海底油探査と開発の仕事に関する技術に関心をもつ技術者を受け入れる用意があります。

この研修セミナーは，この分野の専門技師と，特に海底潜水の経験を持つ人人を対象とし，最も最近の技術に関する講義及び特殊な用具と方法の説明が含まれます。もちろん，潜水経験のある技術者だけが，実際の潜水に参加することを許されます。絶対に安全を確保するという理由から，潜水に参加する技術者は，フランス語に精通していなければなりません。

貴任地国の技師が，このようなセミナーに深い関心を持っていると考えられるかどうか，お知らせ下さい。又，この種の活動の実現化を望む国が多い場合にのみ，このセミナーの時期，参加条件及び詳細のプログラムを示す，いつもの案内状の発送にとりかかりますので，このセミナーのテーマに関する貴見を伺えれば幸いに存じます。

本件について興味をおもちの方は当学会までお申し出ください。

賛 助 会 員

井出利明	釧路市白金町 11
伊藤精機株式会社	東京都千代田区神田神保町 1-65　共益ビル
株式会社内田老鶴圃新社　内田至	東京都千代田区九段 1-2-1
梅林弘直	東京都千代田区大手町 2-4　新大手町ビル7階　極東貿易株式会社
小樽舶用電機株式会社	小樽市色内町 1-20
海上電機株式会社	東京都千代田区神田錦町 1-19
晄東電子株式会社	東京都港区芝新橋 1-30　新幸ビル
協同低温工業株式会社	東京都千代田区神田佐久間町 1-21　山伝ビル
協和商工株式会社	東京都豊島区目白4丁目 24-1
小松川化工機株式会社	東京都江戸川区西小松川 1-2645
株式会社光電製作所	東京都品川区上大崎 2-10-45
小山康三	東京都文京区本駒込 5-13　英和印刷社
株式会社産研	沼津市千本郷林 1907
三信船舶電具株式会社	東京都千代田区内神田 1-15
三洋水路測量株式会社	東京都港区新橋 5-23-7　三栄ビル
シュナイダー財団極東駐在事務所	東京都港区芝琴平町 38　日本ガス協会ビル
昭和電装株式会社	高松市福岡町 467
大洋電機株式会社	東京都千代田区神田錦町 3-16
株式会社鶴見精機工作所	横浜市鶴見区鶴見町 1506
帝国酸素株式会社	神戸市兵庫区高松町 22-1
東京海上火災保険株式会社東京営業第2部	東京都千代田区丸ノ内 3-12
東京工材株式会社	東京都中央区築地 4-2　築三ビル
東京レプ株式会社	東京都豊島区池袋 2-1120　ローズマンション 302 号
株式会社東邦電探	東京都杉並区上高井戸 5-327
株式会社ナック	東京都中央区銀座 1-5-6
日本アクアラング株式会社	東京都豊島区北大塚 1-16-6　大塚ビル
日本海事広報協会海の世界編集部	東京都港区琴平町 35　船舶振興ビル
有限会社日本ダイビングスポーツ	神戸市兵庫区神田町 3
日本テトラポッド株式会社	東京都港区新橋 2-1-13 新橋富士ビル9階
日本無線株式会社	東京都港区芝桜川町 25　第五森ビル
舶用電球株式会社	東京都目黒区下目黒 1-6-21
有限会社ハラダ電機製作所	東京都豊島区池袋 8-3292
ヒエン電工株式会社	堺市松屋町 1-3
深田多満男	東京都港区芝虎ノ門8　虎ノ門実業会館　深田サルベージ株式会社
福永時男	広島市観音町 9-1　福永書店
藤田潔	東京都中央区銀座西 7-6　株式会社ビデオプロモーション
藤田峯雄	東京都江東区南砂 1-3-25　株式会社　中村鉄工所
フランス物産株式会社	東京都千代田区神田錦町 1-6　教文館内
古野電気株式会社	東京都中央区八重洲 4-5　藤和ビル
三菱重工業株式会社	東京都千代田区丸の内 2-10
株式会社吉田製作所	東京都台東区上野 3-13-9
吉野計器製作所	東京都北区西ケ原 1-14
株式会社離合社	東京都千代田区神田鍛冶町 1-2　丸石ビル
株式会社渡部計器製作所	東京都文京区向丘 1-7-17

（50 音順）

うみ(日仏海洋学会誌)

第 7 巻 (1969 年)

総　目　次

第 1 号

第 2 号

La mer (Bulletin de la Société franco-japonaise d'océanographie)

Tome 7 (1969)

Sommaire

Numéro 1

Numéro 2

総　目　次

第 3 号

原　著

寄　稿

総　説

第 4 号

原　著

資　料

Numéro 3

Notes originales

Miscellanées

Compte rendu

Numéro 4

Notes originales

Documentation

ながい経験と最新の技術を誇る！

大洋の船舶用電気機器

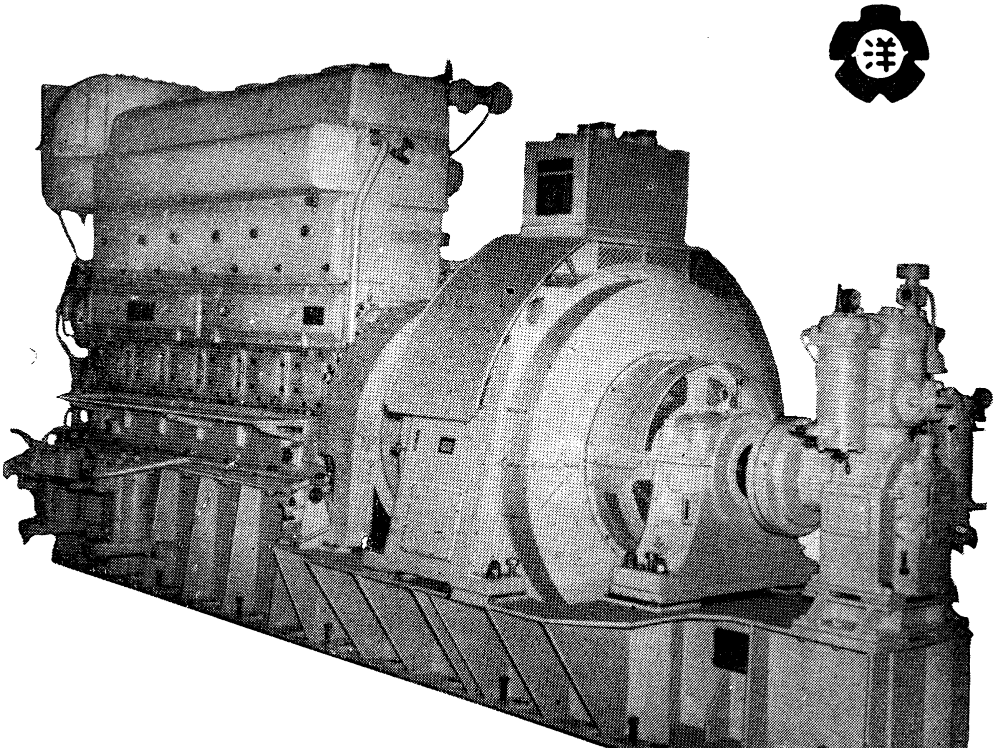

主要生産品目

自励・他励交流発電機
直流発電機
各種電動機及制御装置
船舶自動化装置
配　電　盤

大洋電機株式会社

取締役社長　山田沢三

本　　　社	東京都千代田区神田錦町３の１６ 電話　東京　(293)　３０６１～８
岐阜工場	岐阜県羽島郡笠松町如月町１８ 電話　笠松　４１１～５
伊勢崎工場	群馬県伊勢崎市八斗島町７２６ 電話　伊勢崎 1815・1816・1835・816
下関出張所	下関市竹崎町３９９ 電話　下関　(22) ２８２０・３７０４
北海道出張所	札幌市北二条東二丁目　浜建ビル 電話　札幌 (25) 6347 (23) 8061・8261

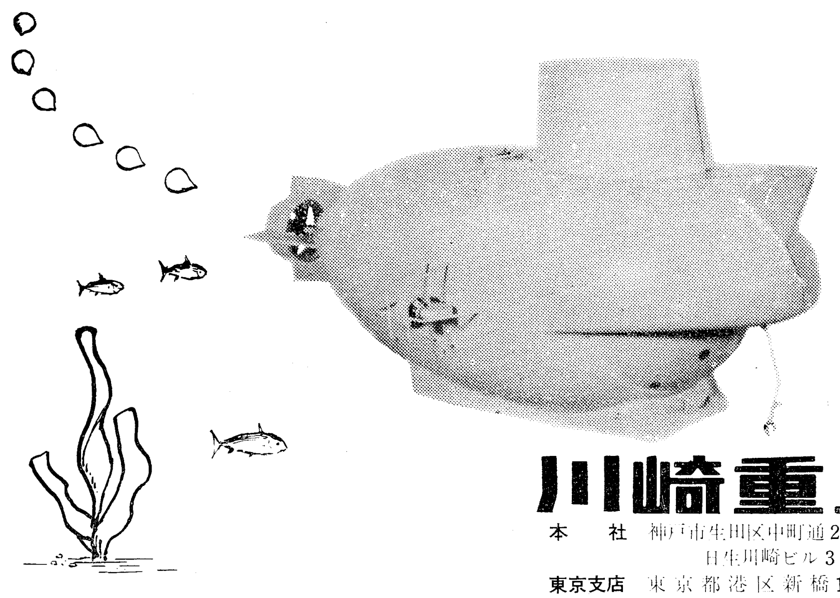

昭和44年11月15日 印刷
昭和44年11月30日 発行　　うみ　第7巻 第4号

定価 ¥400

編集者　今村 豊
発行者　佐々木忠義
発行所　日仏海洋学会
財団法人 日仏会館内
東京都千代田区神田駿河台2-3
郵便番号:101
電話 (291) 1141
振替番号:東京 96503

印刷者　小山康三
印刷所　英和印刷社
東京都文京区本駒込5—13
郵便番号:113
電話 (828) 3935

第7巻　第4号

目　　次

原　　著

資　　料

総 目 次（第7巻）

Tome 7　N° 4

SOMMAIRE

Notes originales

Documentation

Sommaire du Tome 7